

# Recap for SEISMIC RISK: SEISMIC SOURCES

FABIO ROMANELLI

Department of Mathematics & Geosciences

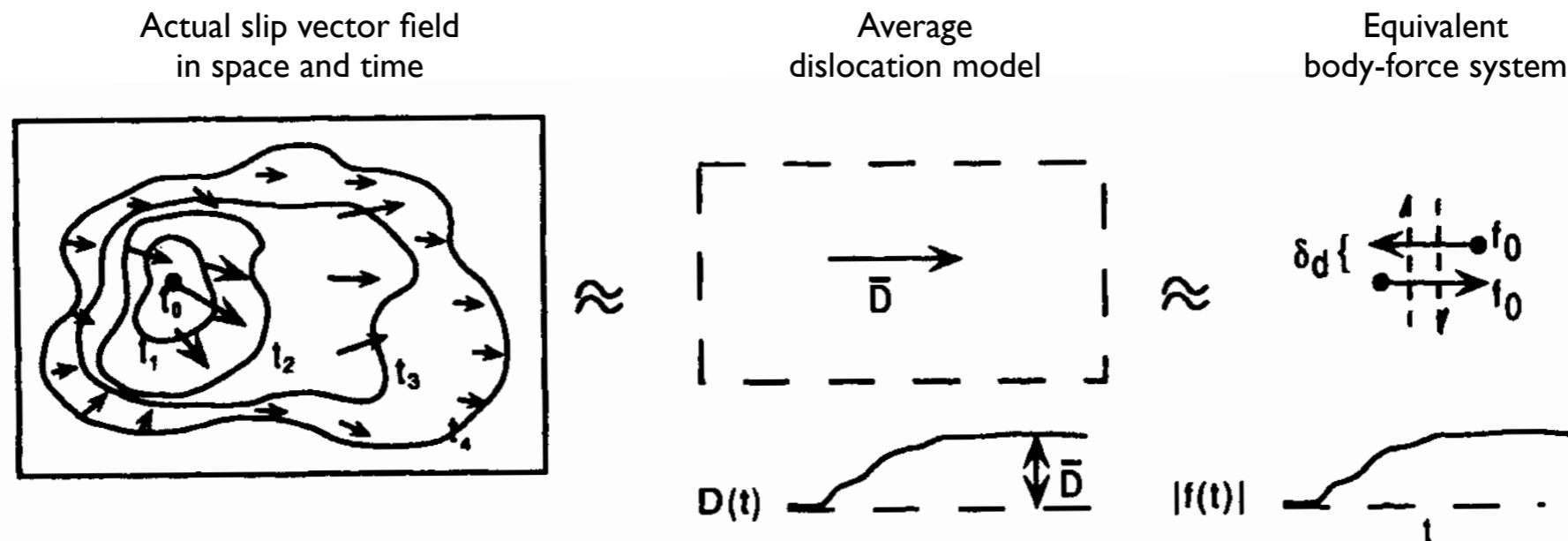
[romanel@units.it](mailto:romanel@units.it)



UNIVERSITÀ  
DEGLI STUDI DI TRIESTE

# Equivalent Forces

The observable seismic radiation is through energy release as the fault surface moves: formation and propagation of a crack. This complex dynamical problem can be studied by kinematical equivalent approaches.



The scope is to develop a representation of the displacement generated in an elastic body in terms of the quantities that originated it: body forces and applied tractions and displacements over the surface of the body.

The actual slip process will be described by superposition of equivalent body forces acting in space (over a fault) and time (rise time).

# Final source representation

$$u_n(\mathbf{x}, t) = \iint_{\Sigma} [u_i] c_{ijpq} v_j * \frac{\partial G_{np}}{\partial \xi_q} d\Sigma$$

$$m_{pq} = [u_i] c_{ijpq} v_j \quad u_n(\mathbf{x}, t) = \iint_{\Sigma} m_{pq} * \frac{\partial G_{np}}{\partial \xi_q} d\Sigma$$

And if the source can be considered a point-source (for distances greater than fault dimensions), the contributions from different surface elements can be considered in phase.

Thus for an effective point source, one can define the moment tensor:

$$M_{pq} = \iint_{\Sigma} m_{pq} d\Sigma$$
$$u_n(\mathbf{x}, t) = M_{pq} * G_{np,q}$$

# Moment tensor decomposition

The moment tensor is symmetric (thus the roles of  $\mathbf{u}$  and  $\mathbf{v}$  can be interchanged without affecting the displacement field, leading to the **fault plane-auxiliary plane ambiguity**), and it can be diagonalized and decomposed in an isotropic and deviatoric part:

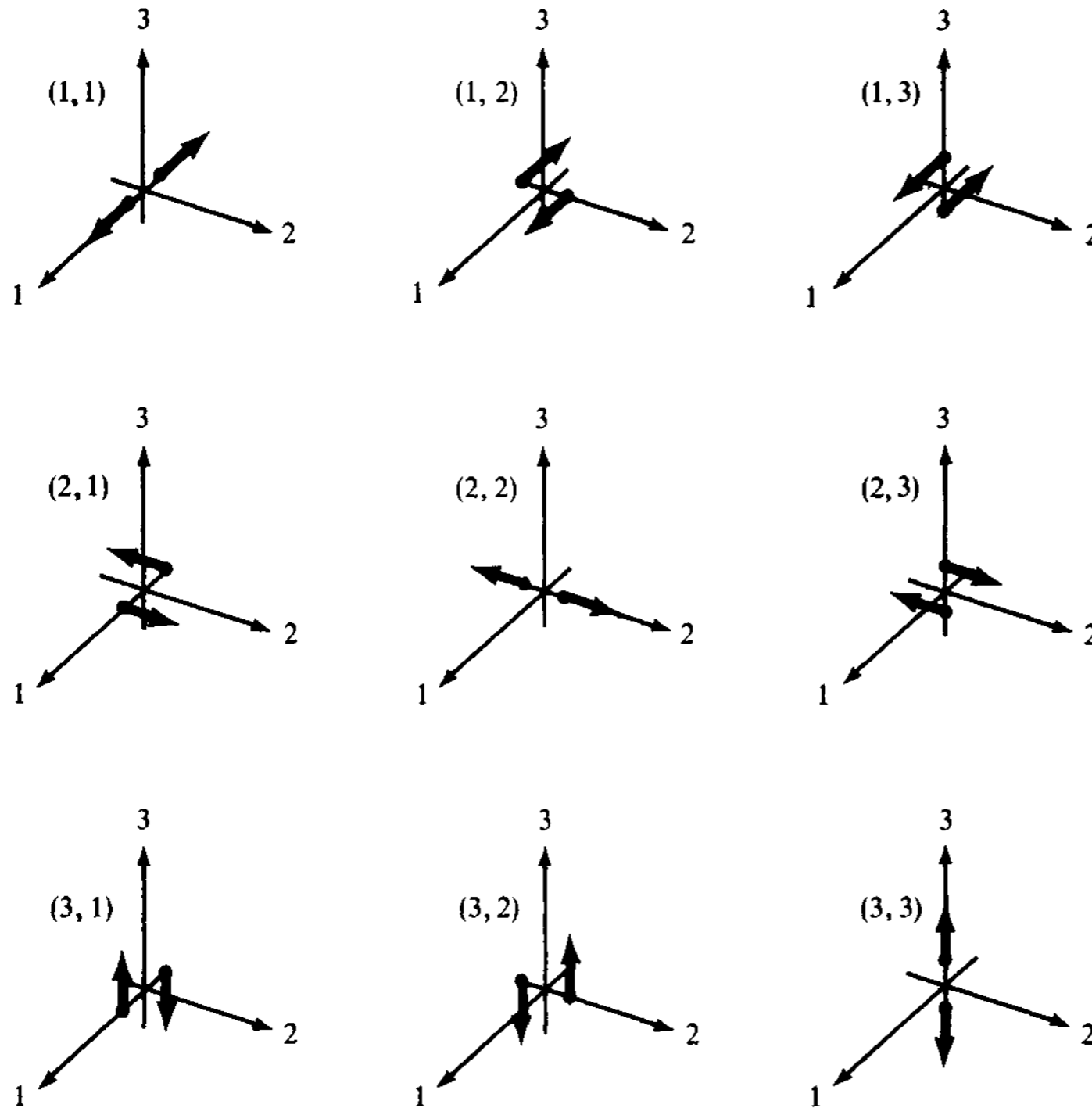
$$M_{pq} = \begin{pmatrix} M_1 & 0 & 0 \\ 0 & M_2 & 0 \\ 0 & 0 & M_3 \end{pmatrix} = \frac{1}{3} \begin{pmatrix} \text{tr}(M) & 0 & 0 \\ 0 & \text{tr}(M) & 0 \\ 0 & 0 & \text{tr}(M) \end{pmatrix} + \begin{pmatrix} M'_1 & 0 & 0 \\ 0 & M'_2 & 0 \\ 0 & 0 & M'_3 \end{pmatrix}$$

For a shear dislocation, the equivalent point force is a **double-couple**, since internal faulting implies that the total force  $\mathbf{f}^{[u]}$  and its total moment are null. The seismic moment has a **null trace** and **one of the eigenvalues is 0**.

$$M_{pq}(\text{doublecouple}) = \begin{pmatrix} M_0 & 0 & 0 \\ 0 & 0 & 0 \\ 0 & 0 & -M_0 \end{pmatrix} \quad \text{with } M_0 = \mu A[\bar{u}]$$

$M_0$  is called **seismic moment**, a scalar quantity related to the area of the fault and to the slip, averaged over the fault plane.

# Moment tensor components

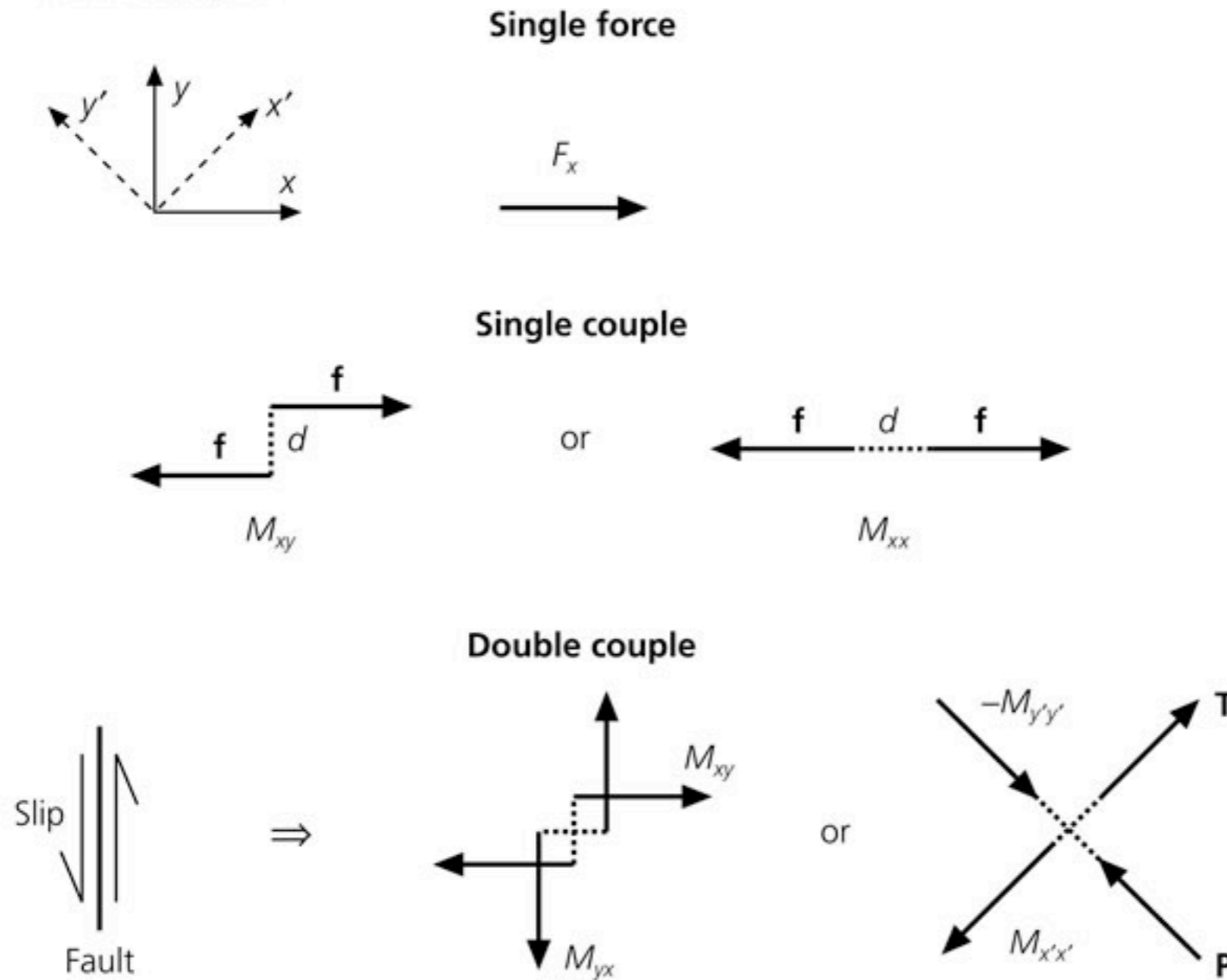


Point sources can be described by the seismic moment tensor  $M_{pq}$ , whose elements have clear physical meaning of **forces acting on particular planes.**

The nine possible couples that are required to obtain equivalent forces for a generally oriented displacement discontinuity in anisotropic media.

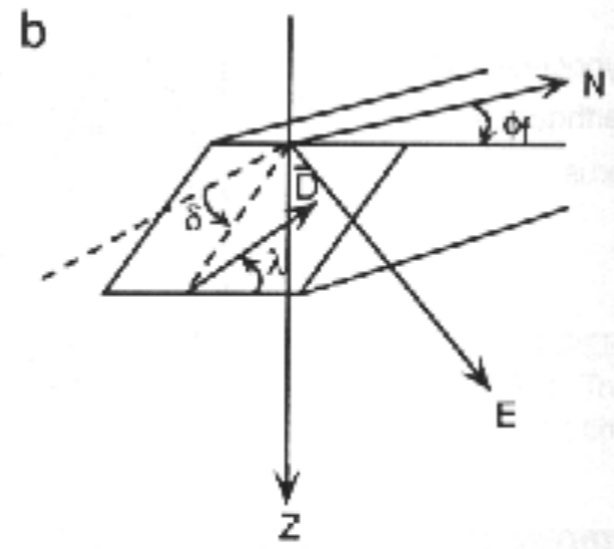
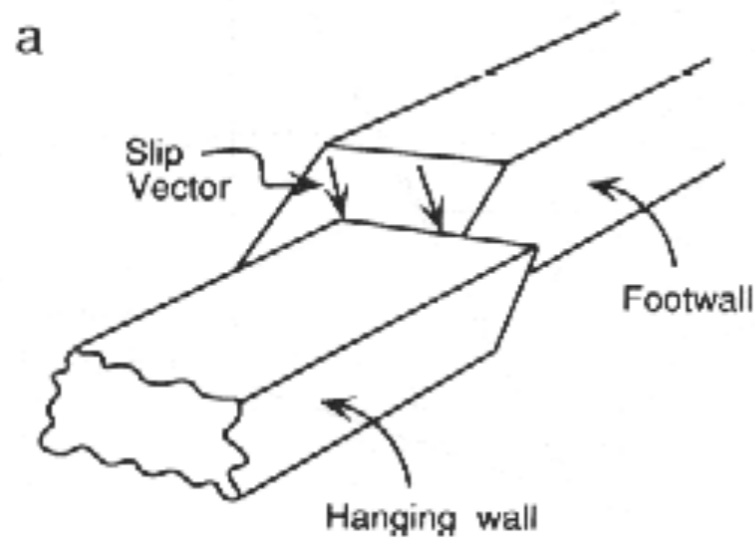
# Moment tensor components

**Figure 4.4-1: Equivalent body forces for a single force, single couple, and double couple.**

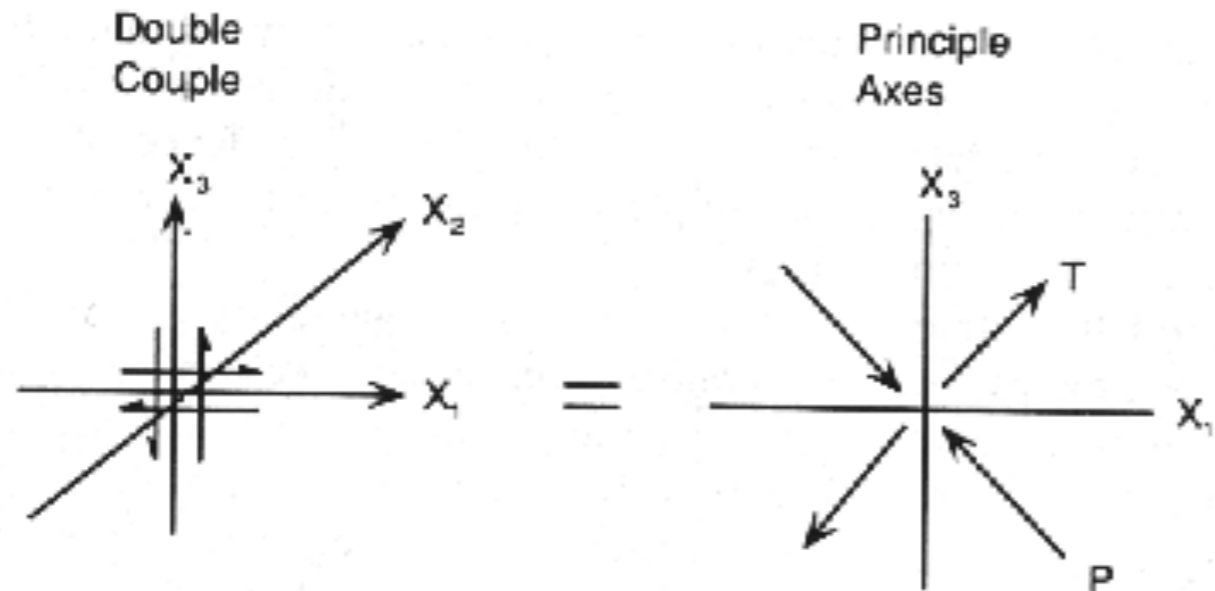


Point sources can be described by the seismic moment tensor  $M_{pq}$ , whose elements have clear physical meaning of **forces acting on particular planes.**

# Angle and axis conventions



Convention for naming blocks, fault plane, and slip vector, i.e. strike, dip and rake



Force system or a double couple in the xz-plane

T and P axes are the directions of maximum positive or negative first break.

# Moment tensor and fault vectors

The orthogonal eigenvectors to the above eigenvalues give the directions of the principal axes:  $\mathbf{b}$ , corresponding to eigenvalue 0, gives the **null-axis**,  $\mathbf{t}$ , corresponding to the positive eigenvalue, gives the **tension axis** (T) and  $\mathbf{p}$  gives the **pressure axis** (P) of the tensor.

They are related to the  $\mathbf{u}$  and  $\mathbf{v}$  vector, defining respectively the slip vector and the fault plane:

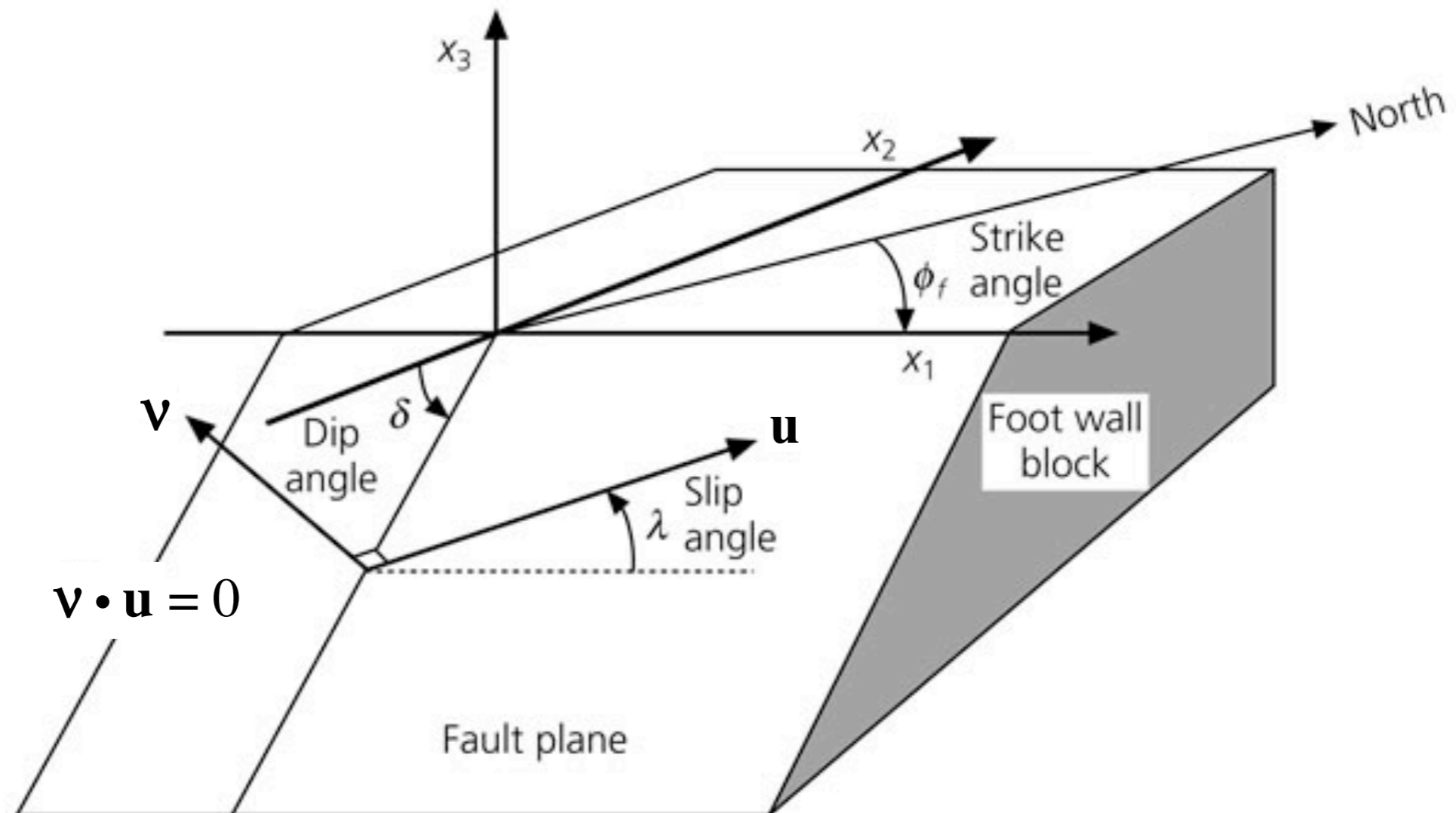
$$\left\{ \begin{array}{l} \mathbf{t} = \frac{1}{\sqrt{2}} (\mathbf{v} + \mathbf{u}) \\ \mathbf{b} = (\mathbf{v} \times \mathbf{u}) \\ \mathbf{p} = \frac{1}{\sqrt{2}} (\mathbf{v} - \mathbf{u}) \end{array} \right. \quad \left\{ \begin{array}{l} \mathbf{u} = \frac{1}{\sqrt{2}} (\mathbf{t} + \mathbf{p}); \frac{1}{\sqrt{2}} (\mathbf{t} - \mathbf{p}) \\ \mathbf{v} = \frac{1}{\sqrt{2}} (\mathbf{t} - \mathbf{p}); \frac{1}{\sqrt{2}} (\mathbf{t} + \mathbf{p}) \end{array} \right.$$



# Moment tensor and fault plane solution

$$\mathbf{u} = \begin{cases} [\bar{u}] (\cos \lambda \cos \phi + \cos \delta \sin \lambda \sin \phi) \hat{\mathbf{e}}_x \\ [\bar{u}] (\cos \lambda \sin \phi - \cos \delta \sin \lambda \cos \phi) \hat{\mathbf{e}}_y \\ [\bar{u}] (-\sin \delta \sin \lambda) \hat{\mathbf{e}}_z \end{cases} \quad \mathbf{v} = \begin{cases} (-\sin \delta \sin \phi) \hat{\mathbf{e}}_x \\ (-\sin \delta \cos \phi) \hat{\mathbf{e}}_y \\ (-\cos \delta) \hat{\mathbf{e}}_z \end{cases}$$

Figure 4.2-2: Fault geometry used in earthquake studies.



# Moment tensor and fault plane solution

The slip vector and the fault normal can be expressed in terms of strike ( $\varphi$ ), dip ( $\delta$ ) and rake ( $\lambda$ ):

$$\mathbf{u} = \begin{cases} [\bar{u}] (\cos \lambda \cos \phi + \cos \delta \sin \lambda \sin \phi) \hat{\mathbf{e}}_x \\ [\bar{u}] (\cos \lambda \sin \phi - \cos \delta \sin \lambda \cos \phi) \hat{\mathbf{e}}_y \\ [\bar{u}] (-\sin \delta \sin \lambda) \hat{\mathbf{e}}_z \end{cases} \quad \mathbf{v} = \begin{cases} (-\sin \delta \sin \phi) \hat{\mathbf{e}}_x \\ (-\sin \delta \cos \phi) \hat{\mathbf{e}}_y \\ (-\cos \delta) \hat{\mathbf{e}}_z \end{cases}$$

Then the Cartesian components of the symmetric moment tensor can be written as:

$$\begin{aligned} M_{xx} &= -M_0 (\sin \delta \cos \lambda \sin 2\phi + \sin 2\delta \sin \lambda \sin^2 \phi) & M_{xy} &= M_0 (\sin \delta \cos \lambda \sin 2\phi + 0.5 \sin 2\delta \sin \lambda \sin 2\phi) \\ M_{yy} &= M_0 (\sin \delta \cos \lambda \sin 2\phi - \sin 2\delta \sin \lambda \cos^2 \phi) & M_{xz} &= -M_0 (\cos \delta \cos \lambda \cos \phi + \cos 2\delta \sin \lambda \sin \phi) \\ M_{zz} &= M_0 (\sin 2\delta \sin \lambda) & M_{yz} &= -M_0 (\cos \delta \cos \lambda \sin \phi - \cos 2\delta \sin \lambda \cos \phi) \end{aligned}$$

# Solution for elastodynamic GF

We have to a) solve the wave equation for the Lamè potentials of body force and then b) to calculate the displacement.

After some heavy algebra (Stokes, 1849), generalizing from the  $x_j$  direction and using direction cosines ( $\gamma_i = x_i/r = \partial r/\partial x_i$ )

$$u_i = X_0(t) * G_{ij} =$$

$$= \frac{(3\gamma_i\gamma_j - \delta_{ij})}{4\pi\rho|\mathbf{x}|^3} \int_{|\mathbf{x}|/\alpha}^{|\mathbf{x}|/\beta} \tau X_0(t-\tau) d\tau +$$

Near field term

$$+ \frac{\gamma_i\gamma_j}{4\pi\rho\alpha^3|\mathbf{x}|} X_0\left(t - \frac{|\mathbf{x}|}{\alpha}\right) +$$

$$+ \frac{(3\gamma_i\gamma_j - \delta_{ij})}{4\pi\rho\beta^3|\mathbf{x}|} X_0\left(t - \frac{|\mathbf{x}|}{\beta}\right)$$

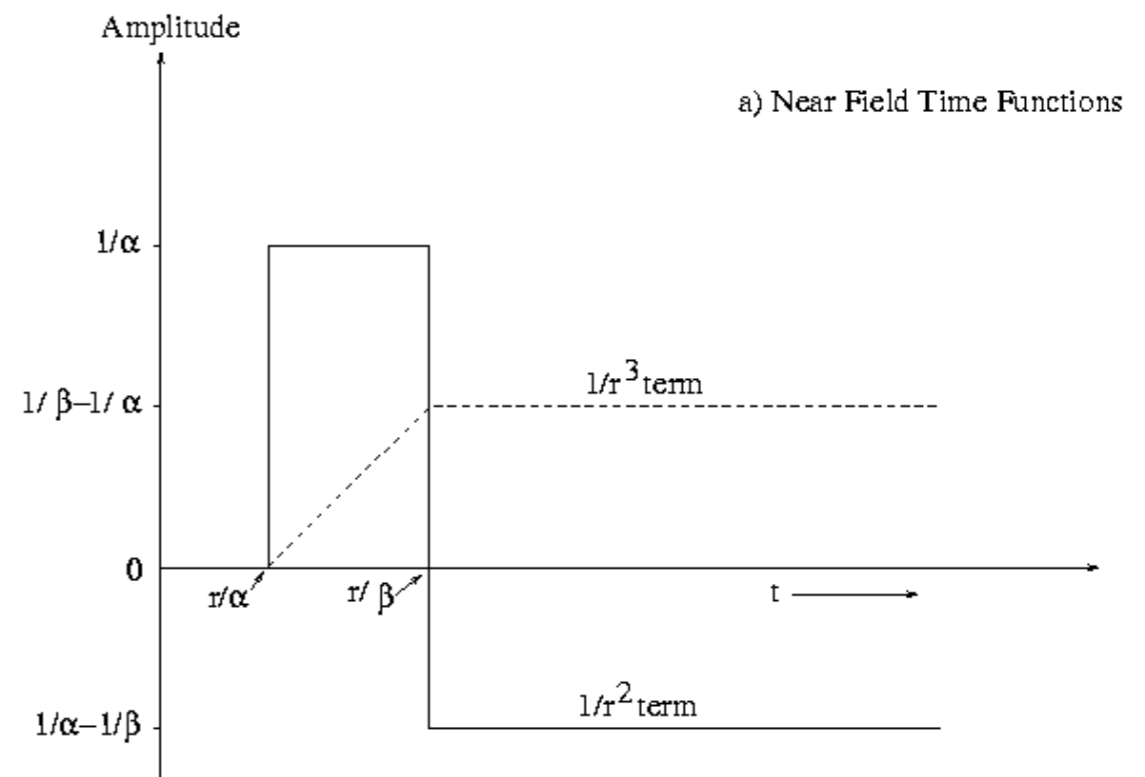
Far field term

# Near field term

The near-field expression of the point force delta function GF is:

$$u_i^{NF} = \frac{(3\gamma_i\gamma_j - \delta_{ij})}{4\pi\rho}$$

$$\left\{ \frac{1}{r^3} \left[ \left(t - \frac{r}{\alpha}\right) H\left(t - \frac{r}{\alpha}\right) - \left(t - \frac{r}{\beta}\right) H\left(t - \frac{r}{\beta}\right) \right] + \frac{1}{r^2} \left[ \frac{1}{\alpha} H\left(t - \frac{r}{\alpha}\right) - \frac{1}{\beta} H\left(t - \frac{r}{\beta}\right) \right] \right\}$$



and the response has a **static** (time-independent) component that corresponds to a permanent deformation of the medium, both in radial and transverse directions.

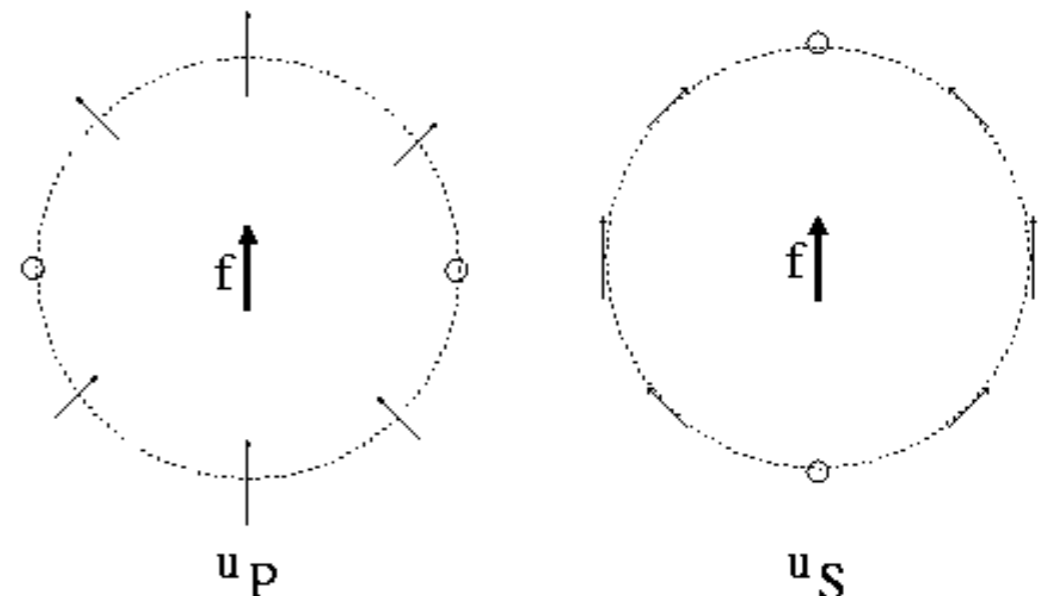
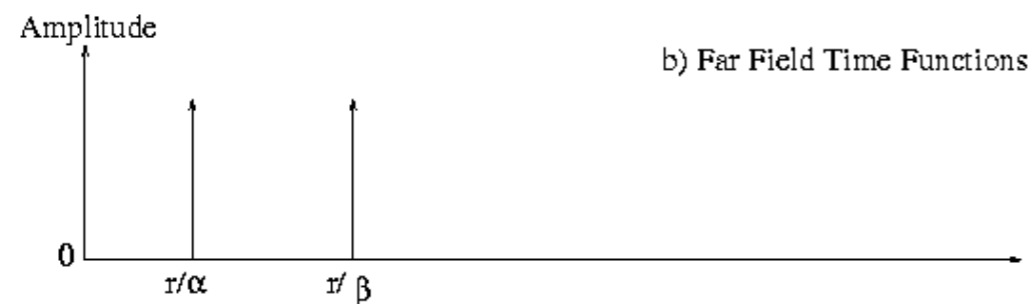
# Far field term

The far-field expressions of the point force delta function GF are characterized by:

- 1) decay as  $1/r$ ;
- 2) are made of P and S waves;
- 3) the displacement waveform is proportional to the applied force at the retarded time;
- 4) have a radiation pattern

$$\left| u_P^{FF} \right| \propto \gamma_1 \gamma_j = \cos\theta$$

$$\left| u_S^{FF} \right| \propto -\gamma_j' = \sin\theta$$



# GF for double couple (DC)

An important case to consider in detail is the radiation pattern expected when the source is a double-couple. The result for a moment time function  $M_0(t)$  is:

$$\begin{aligned}
 u = & \frac{A^{NF}}{4\pi\rho|\mathbf{x}|^4} \int_{|\mathbf{x}|/\beta}^{|\mathbf{x}|/\alpha} \tau M_0(t-\tau) d\tau + \\
 & + \frac{A_P^{IF}}{4\pi\rho\alpha^2|\mathbf{x}|^2} M_0\left(t - \frac{|\mathbf{x}|}{\alpha}\right) - \frac{A_S^{IF}}{4\pi\rho\beta^2|\mathbf{x}|^2} M_0\left(t - \frac{|\mathbf{x}|}{\beta}\right) + \\
 & + \frac{A_P^{FF}}{4\pi\rho\alpha^3|\mathbf{x}|} \dot{M}_0\left(t - \frac{|\mathbf{x}|}{\alpha}\right) - \frac{A_S^{FF}}{4\pi\rho\beta^3|\mathbf{x}|} \dot{M}_0\left(t - \frac{|\mathbf{x}|}{\beta}\right)
 \end{aligned}$$

$$A^{NF} = 9\sin 2\theta \cos \phi \hat{\mathbf{r}} - 6 \left( \cos 2\theta \cos \phi \hat{\boldsymbol{\theta}} - \cos \theta \sin \phi \hat{\boldsymbol{\phi}} \right)$$

$$A_P^{IF} = 4\sin 2\theta \cos \phi \hat{\mathbf{r}} - 2 \left( \cos 2\theta \cos \phi \hat{\boldsymbol{\theta}} - \cos \theta \sin \phi \hat{\boldsymbol{\phi}} \right)$$

$$A_S^{IF} = -3\sin 2\theta \cos \phi \hat{\mathbf{r}} + 3 \left( \cos 2\theta \cos \phi \hat{\boldsymbol{\theta}} - \cos \theta \sin \phi \hat{\boldsymbol{\phi}} \right)$$

$$A_P^{FF} = \sin 2\theta \cos \phi \hat{\mathbf{r}}$$

$$A_S^{FF} = \cos 2\theta \cos \phi \hat{\boldsymbol{\theta}} - \cos \theta \sin \phi \hat{\boldsymbol{\phi}}$$

Near field term

Intermediate field term

Far field term

# NF DC (static) Radiation pattern

The static final displacement for a shear dislocation of strength  $M_0$  is:

$$\mathbf{u} = \frac{M_0(\infty)}{4\pi\rho|\mathbf{x}|^2} \left[ \mathbf{A}^{\text{NF}} \left( \frac{1}{2\beta^2} - \frac{1}{2\alpha^2} \right) + \frac{\mathbf{A}_P^{\text{IF}}}{\alpha^2} + \frac{\mathbf{A}_S^{\text{IF}}}{\beta^2} \right] =$$

$$= \frac{M_0(\infty)}{4\pi\rho|\mathbf{x}|^2} \left[ \left( \frac{3}{2\beta^2} - \frac{1}{2\alpha^2} \right) \sin 2\theta \cos \phi \hat{\mathbf{r}} + \frac{1}{\alpha^2} \left( \cos 2\theta \cos \phi \hat{\boldsymbol{\theta}} - \cos \theta \sin \phi \hat{\boldsymbol{\phi}} \right) \right]$$

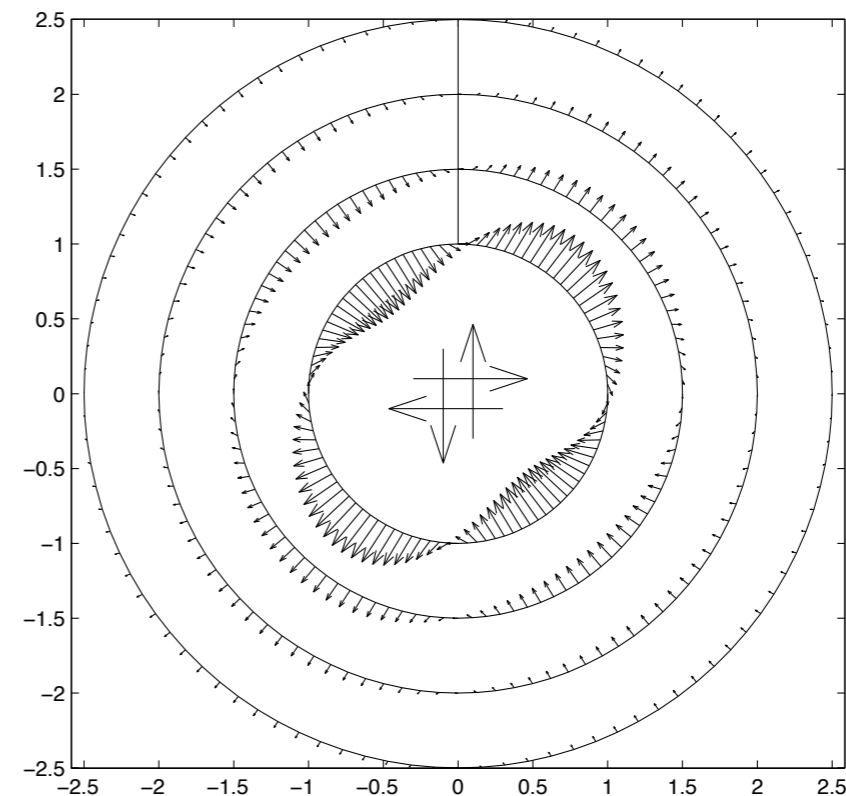
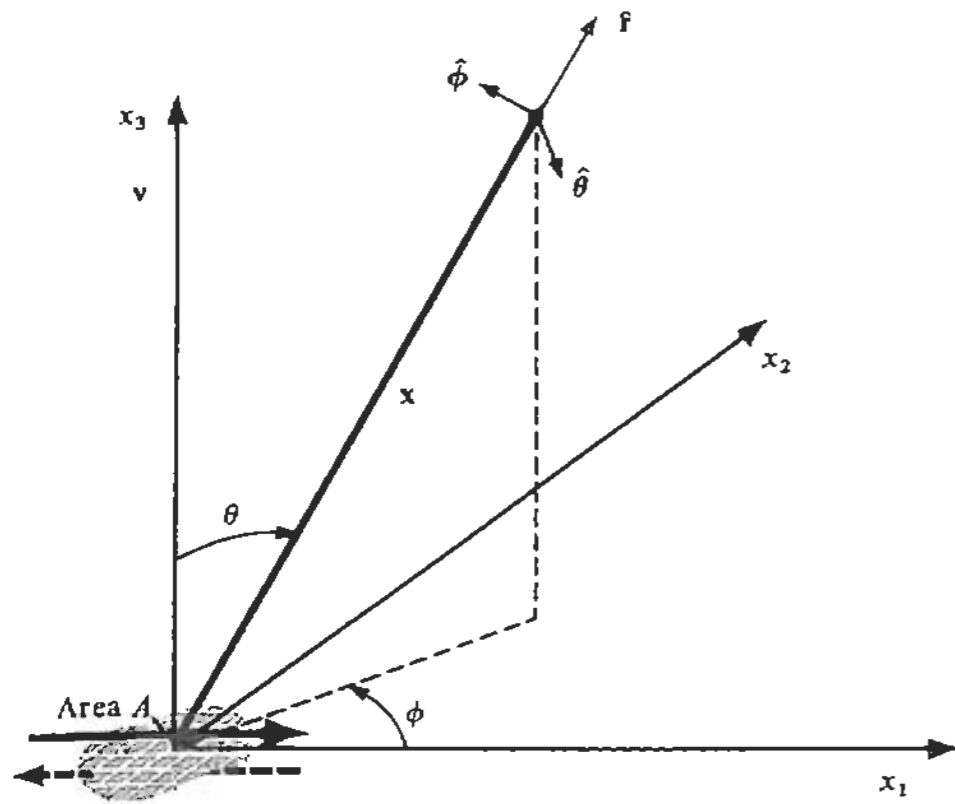
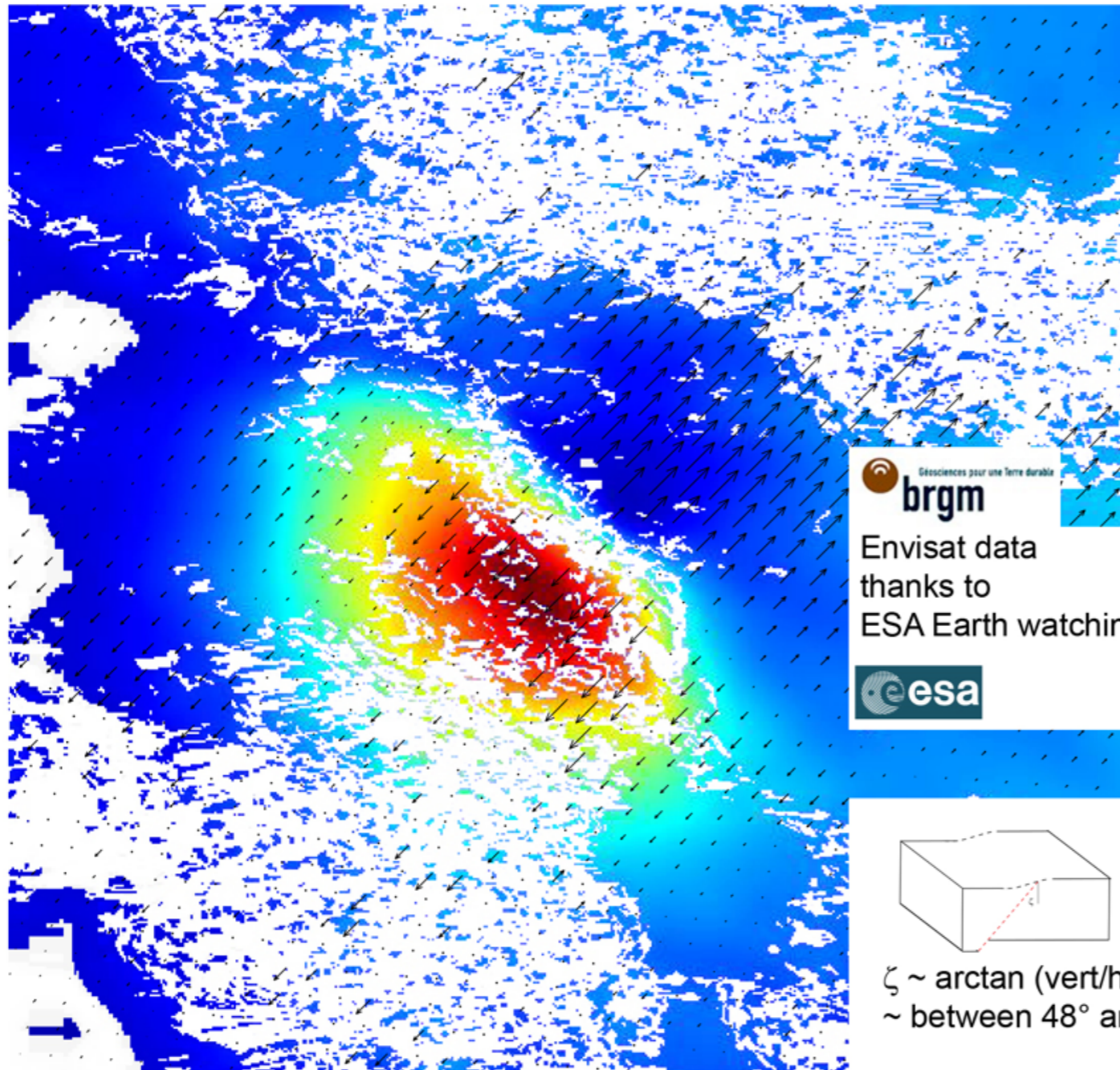



Figure 7: Near-field Static Displacement Field From a Point Double Couple Source ( $\phi = 0$  plane);  $\alpha = 3^{1/2}$ ,  $\beta = 1$ ,  $r = 0.1, 0.15, 0.20, 0.25$ ,  $\rho = 1/4\pi$ ,  $M_\infty = 1$ ; self-scaled displacements

# Coseismic deformation

L'Aquila (Italy) earthquake, Mw 6.3.  
 Horizontal and Vertical surface displacement from InSAR Data  
 (assuming horizontal displacement is perpendicular to the fault strike ~N48W).

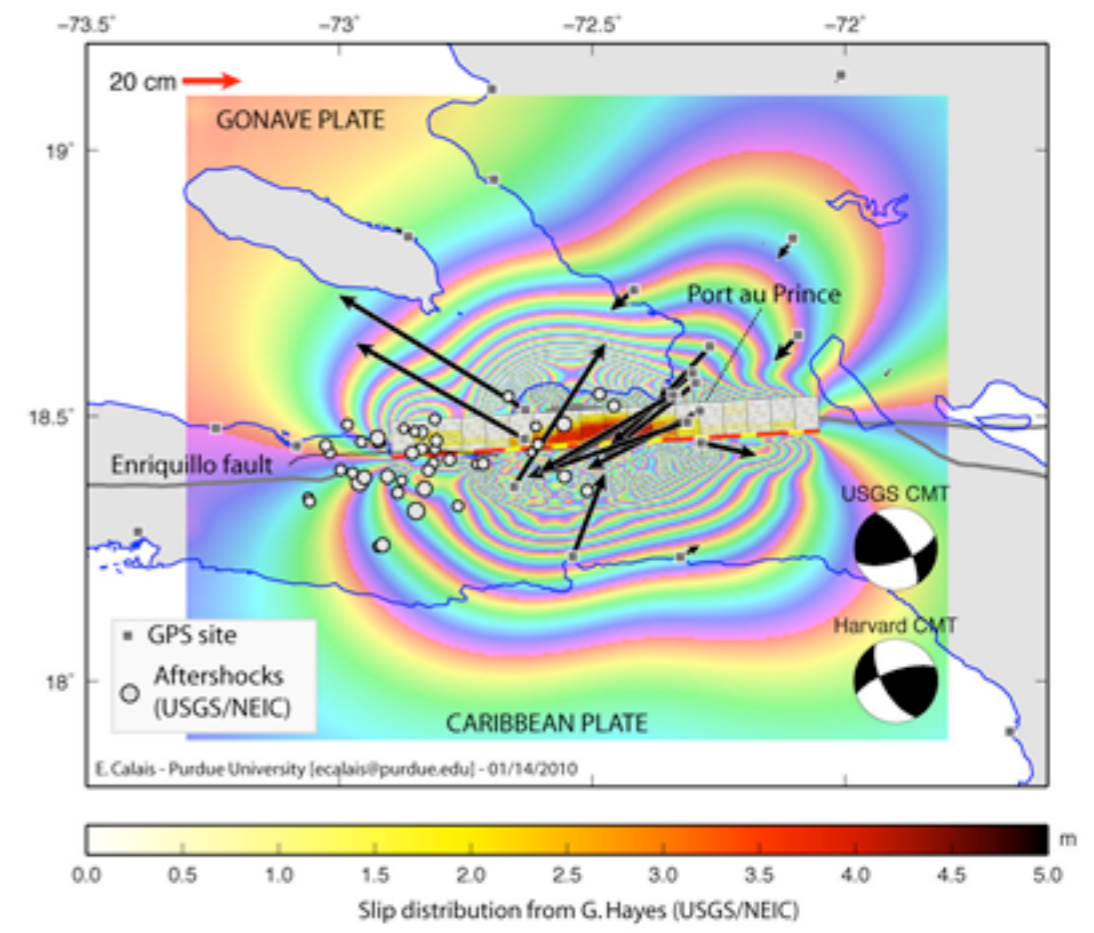



 Géosciences pour une Terre durable  
**brgm**  
 Envisat data  
 thanks to  
 ESA Earth watching Team  

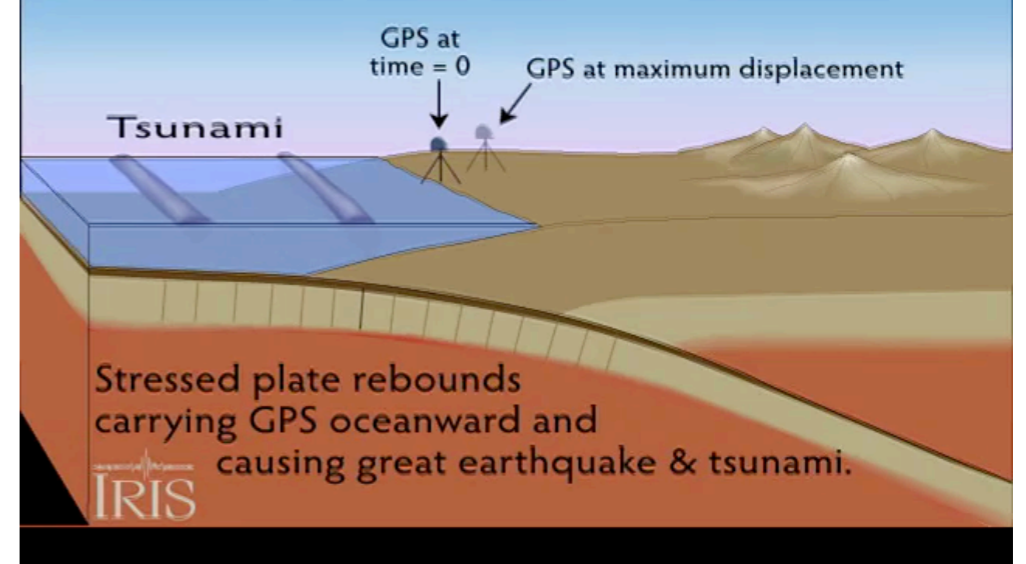

  
 $\zeta \sim \arctan(\text{vert}/\text{horiz})$   
 $\sim \text{between } 48^\circ \text{ and } 51^\circ$

 ~13 cm (horizontal)  
 +2 cm (vertical) -24

SIMULATED COSEISMIC GROUND DEFORMATION  
 HAITI - Mw=7.1 - January 12, 2010

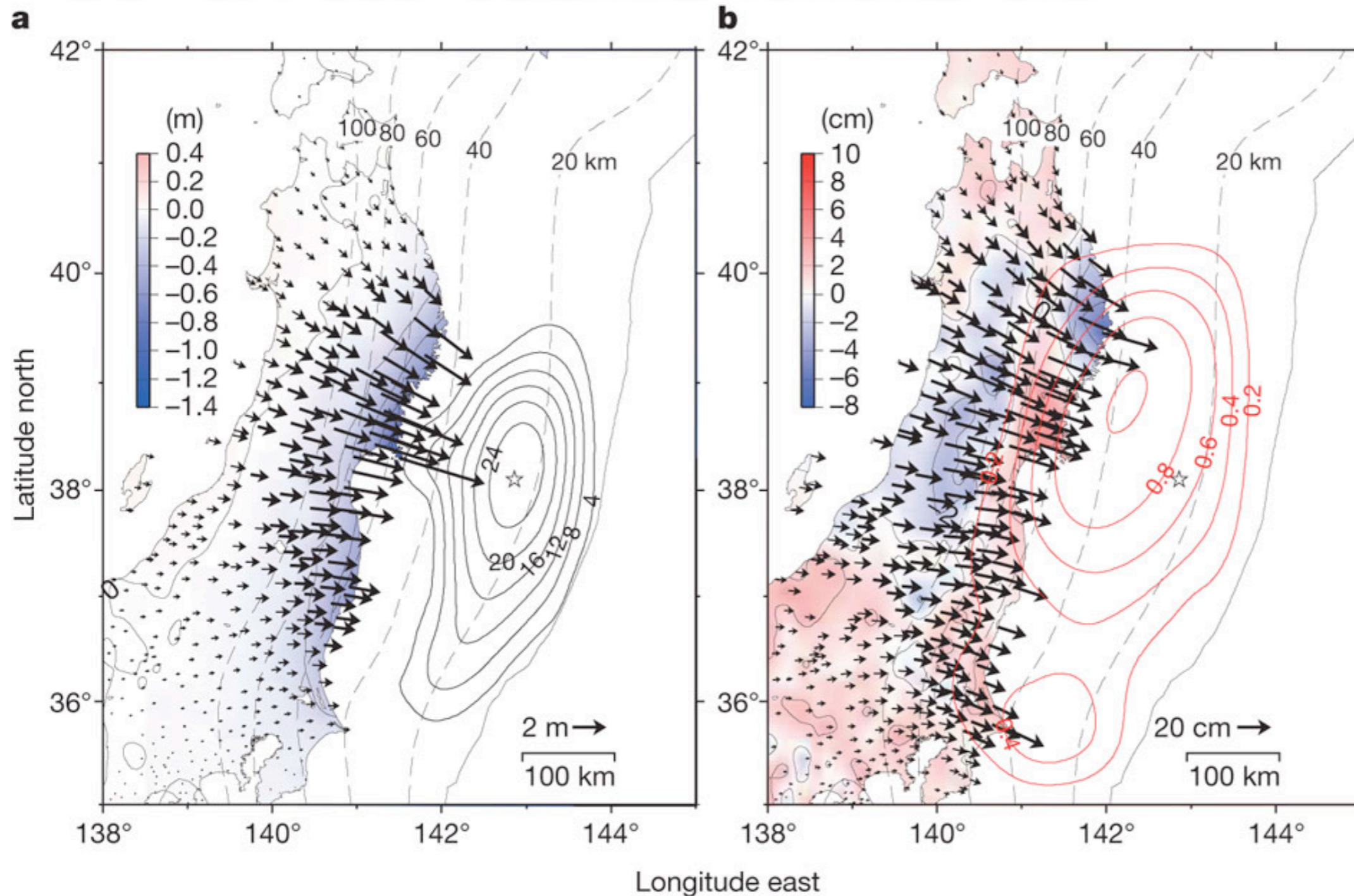


How does land jump with an earthquake?  
 Evidence from GPS stations above subduction zone





# Co- & Post- seismic: Tohoku-oki



a, Coseismic displacements for 10–11 March 2011, relative to the Fukue site. The black arrows indicate the horizontal coseismic movements of the GPS sites. The colour shading indicates vertical displacement. The star marks the location of the earthquake epicentre. The dotted lines indicate the isodepth contours of the plate boundary at 20-km intervals. The solid contours show the coseismic slip distribution in metres.

b, Postseismic displacements for 12–25 March 2011, relative to the Fukue site. The red contours show the afterslip distribution in metres. All other markings represent the same as in a.

# Far field for a DC point source

From the representation theorem we have:  $u_n(\mathbf{x}, t) = M_{pq} * G_{np,q}$

that, in the far field and in a spherical coordinate system becomes:

$$u(\mathbf{x}, t) = \frac{1}{4\pi\rho\alpha^3} \left( \sin 2\theta \cos \phi \hat{\mathbf{r}} \right) \frac{\dot{M}(t - r/\alpha)}{r} + \frac{1}{4\pi\rho\beta^3} \left( \cos 2\theta \cos \phi \hat{\boldsymbol{\theta}} - \cos \theta \sin \phi \hat{\boldsymbol{\phi}} \right) \frac{\dot{M}(t - r/\beta)}{r}$$

and both P and S radiation fields are proportional to the time derivative of the moment function (moment rate). If the moment function is a ramp of duration  $\tau$  (**rise time**), the propagating disturbance in the far-field will be a **boxcar**, with the same duration, and whose amplitude is varying depending on the radiation pattern.

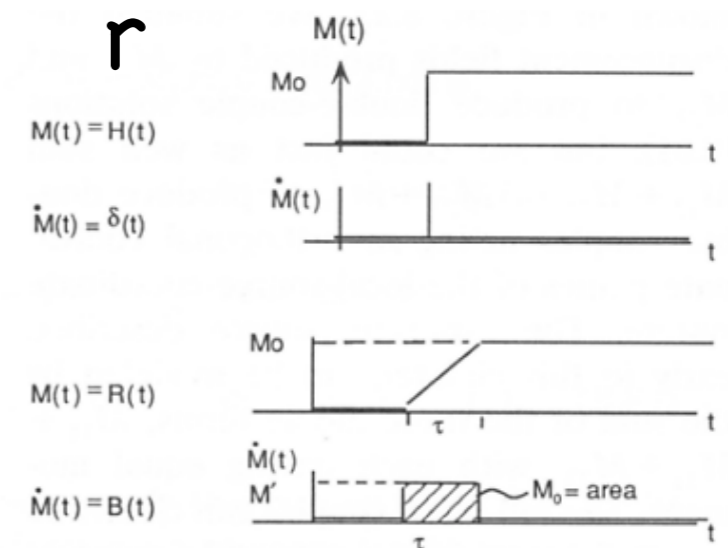


**FIGURE 8.21** Far-field *P*- and *S*-wave displacements are proportional to  $\dot{M}(t)$ , the time derivative of the moment function  $M(t) = \mu A(t)D(t)$ . Simple step and ramp moment functions generate far-field impulses or boxcar ground motions.

# FF DC Radiation pattern

FIGURE 4.5

Diagrams for the radiation pattern of the radial component of displacement due to a double couple, i.e.,  $\sin 2\theta \cos \phi \hat{r}$ . (a) The lobes are a locus of points having a distance from the origin that is proportional to  $\sin 2\theta$ . The diagram is for a plane of constant azimuth, and the pair of arrows at the center denotes the shear dislocation. Note the alternating quadrants of inward and outward directions. In terms of far-field  $P$ -wave displacement, plus signs denote outward displacement (if  $\dot{M}_0(t - r/\alpha)$  is positive), and minus signs denote inward displacement. (b) View of the radiation pattern over a sphere centered on the origin. Plus and minus signs of various sizes denote variation (with  $\theta, \phi$ ) of outward and inward motions. The fault plane and the auxiliary plane are nodal lines (on which  $\sin 2\theta \cos \phi = 0$ ). An equal-area projection has been used (see Fig. 4.17). Point  $P$  marks the pressure axis, and  $T$  the tension axis.

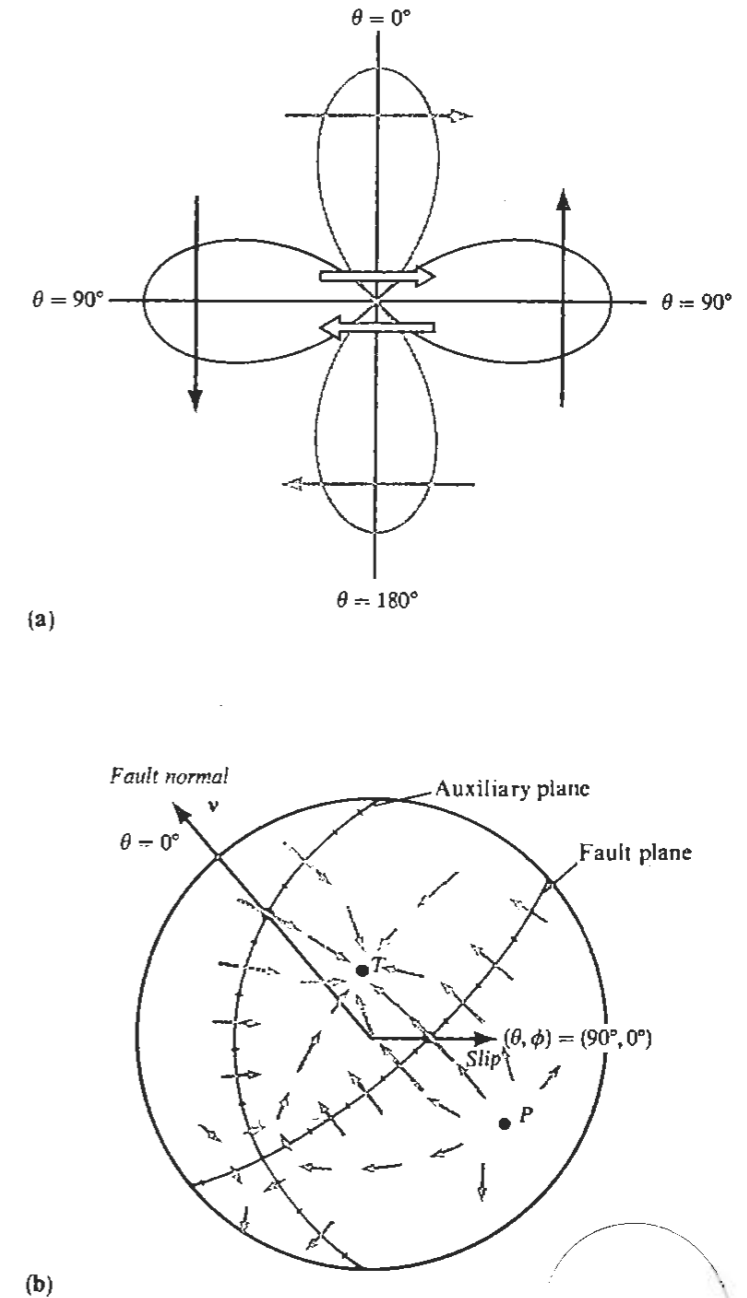
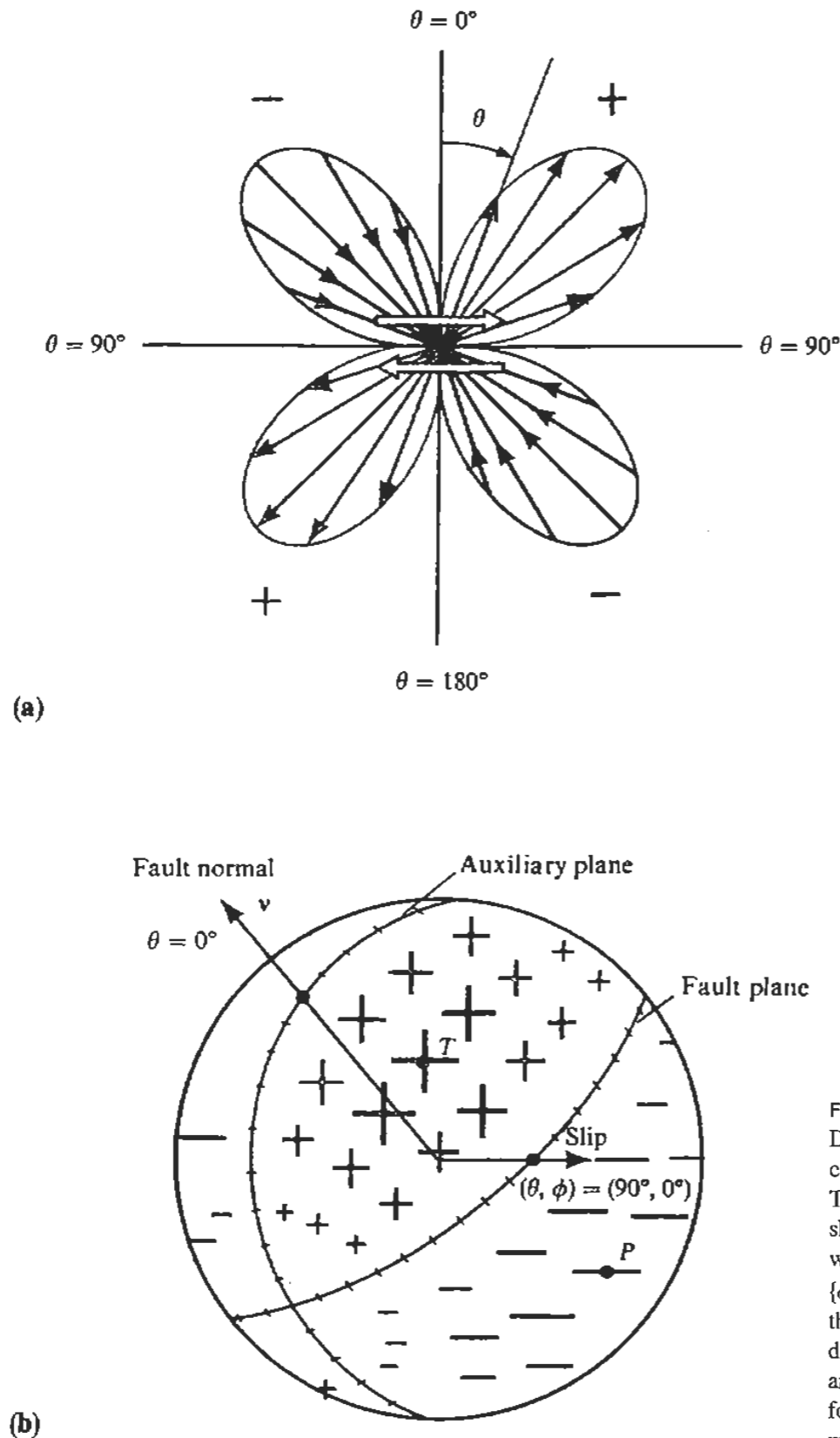
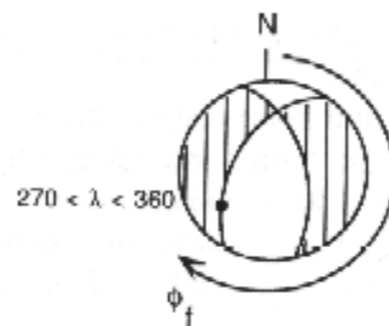
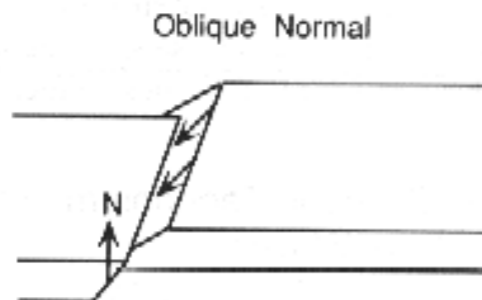
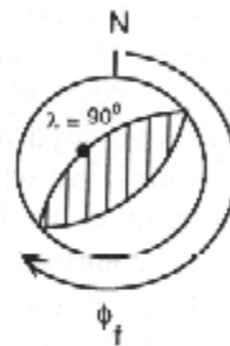
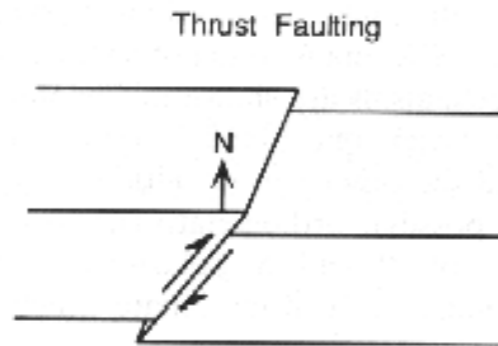
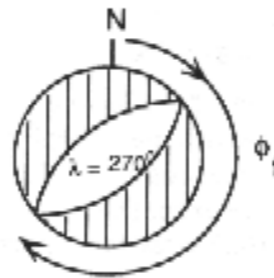
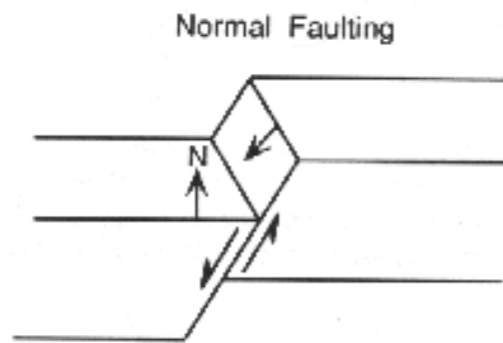
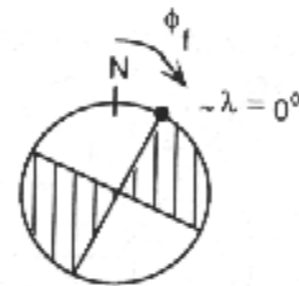
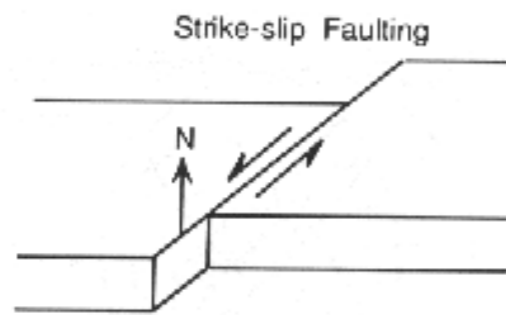


FIGURE 4.6

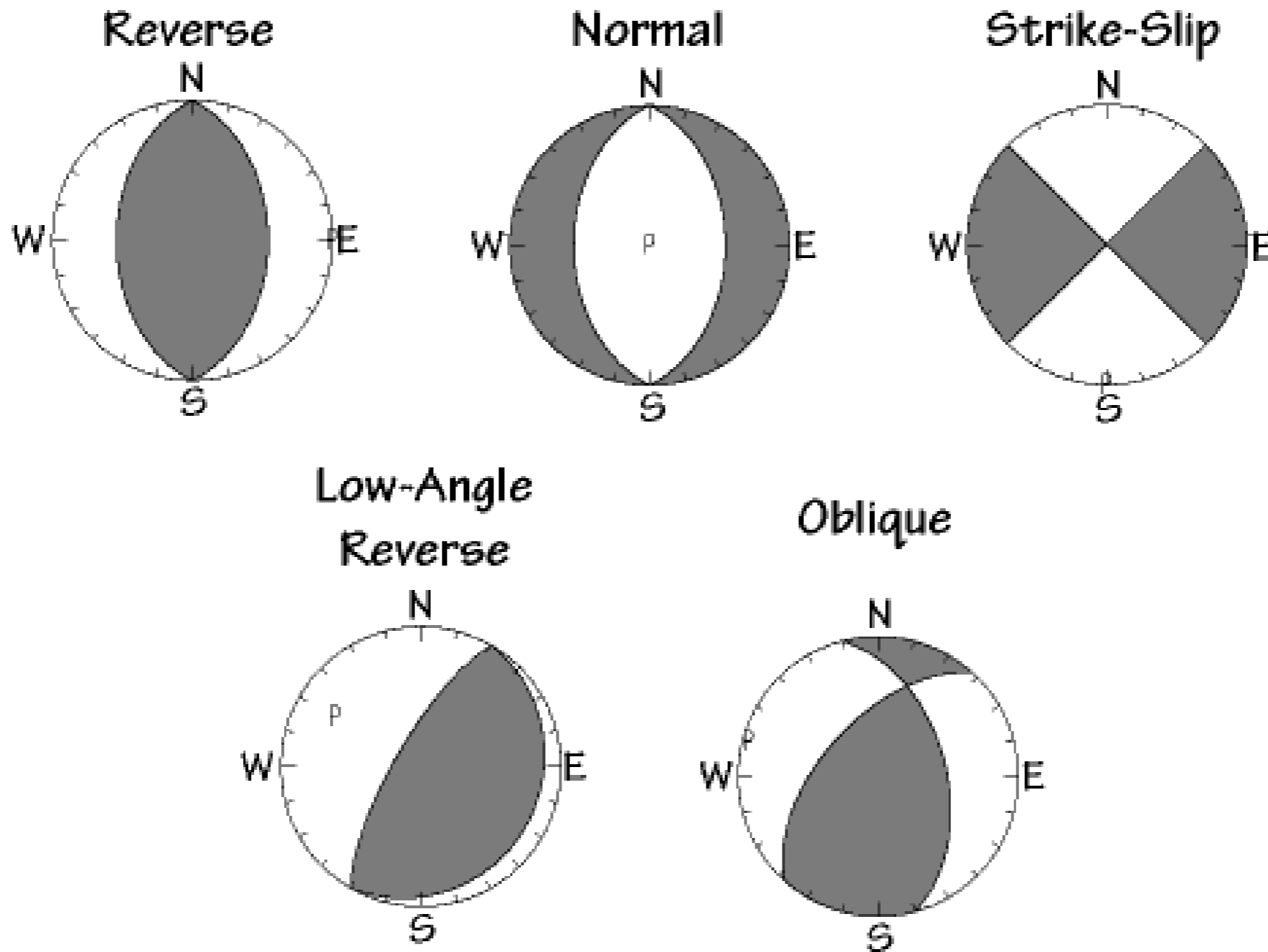
Diagrams for the radiation pattern of the transverse component of displacement due to a double couple, i.e.,  $\cos 2\theta \cos \phi \hat{\theta} - \cos \theta \sin \phi \hat{\phi}$ . (a) The four-lobed pattern in plane  $\{\phi = 0, \phi = \pi\}$ . The central pair of arrows shows the sense of shear dislocation, and arrows imposed on each lobe show the direction of particle displacement associated with the lobe. If applied to the far-field  $S$ -wave displacement, it is assumed that  $\dot{M}_0(t - r/\beta)$  is positive. (b) Off the two planes  $\theta = \pi/2$  and  $\{\phi = 0, \phi = \pi\}$ , the  $\hat{\phi}$  component is nonzero, hence (a) is of limited use. This diagram is a view of the radiation pattern over a whole sphere centered on the origin, and arrows (with varying size and direction) in the spherical surface denote the variation (with  $\theta, \phi$ ) of the transverse motions. There are no nodal lines (where there is zero motion), but nodal points do occur. Note that the nodal point for transverse motion at  $(\theta, \phi) = (45^\circ, 0)$  is a maximum in the radiation pattern for longitudinal motion (Fig. 4.5b). But the maximum transverse motion (e.g., at  $\theta = 0$ ) occurs on a nodal line for the longitudinal motion. The stereographic projection has been used (see Fig. 4.16). It is a conformal projection, meaning that it preserves the angles at which curves intersect and the shapes of small regions, but it does not preserve relative areas.

# Fault types and focal mechanisms



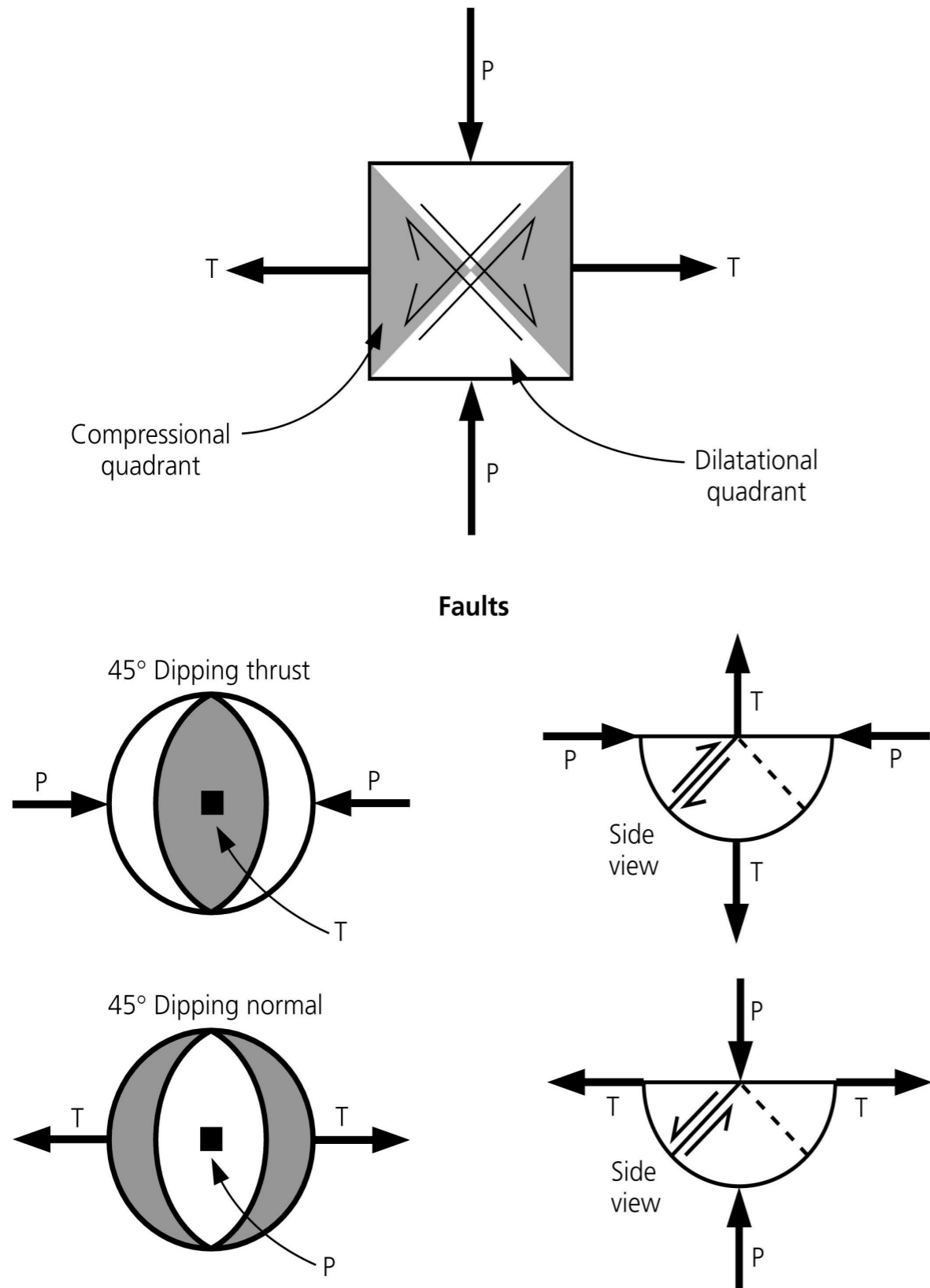
Basis fault types and their appearance in the focal mechanisms. Dark regions indicate compressional P-wave motion.

# The Principal Mechanisms

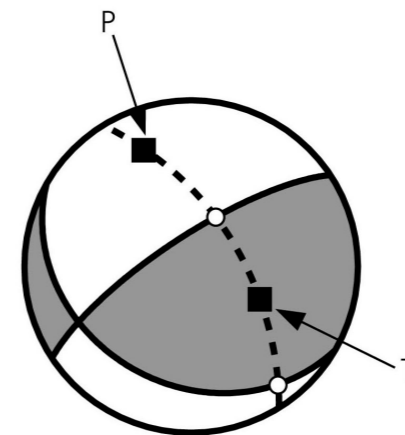


# FM & stress axes

Figure 4.2-16: Relation between fault planes and stress axes.



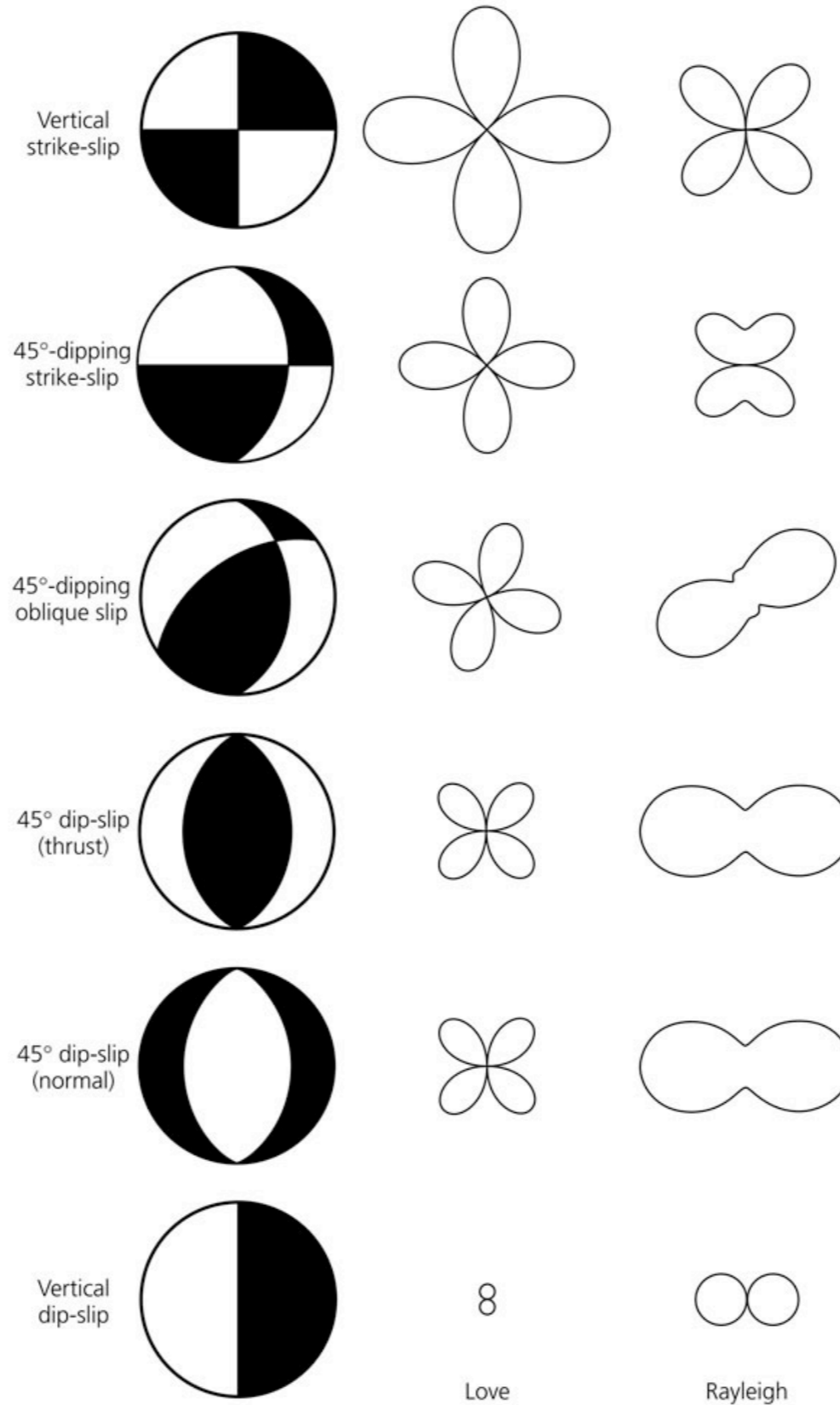
To obtain P and T axes:



On the meridian connecting the poles, the points half-way between the nodal planes are the **P** and **T** axes

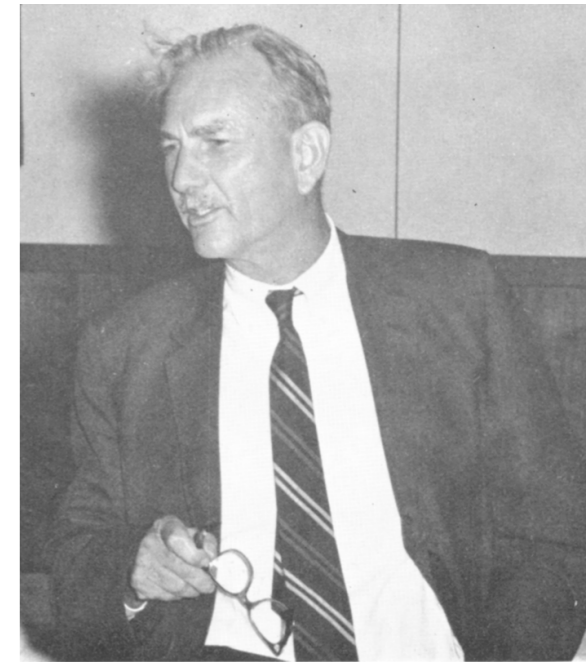
# DC Radiation pattern & surface waves

Figure 4.3-12: Surface wave amplitude radiation patterns for several focal mechanisms.



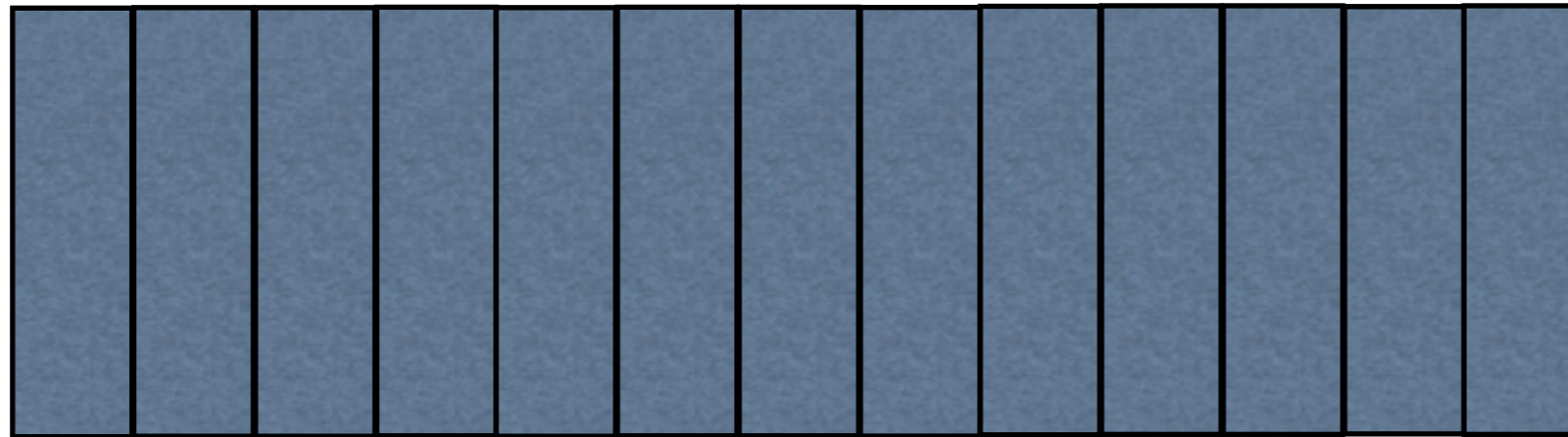
# Haskell dislocation model

Haskell N. A. (1964). Total energy spectral density of elastic wave radiation from propagating faults, Bull. Seism. Soc. Am. 54, 1811-1841

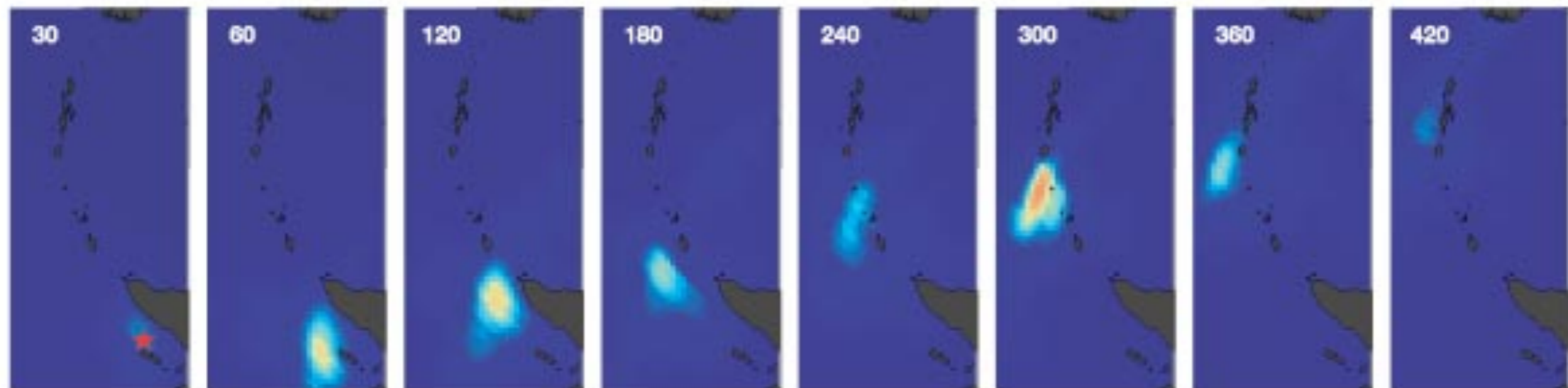


NORMAN A. HASKELL

Rupture →



Sumatra earthquake, Dec 28, 2004



Ishii et al., Nature 2005 doi:10.1038/nature03675



# Haskell source model: far field

For a single segment (point source)

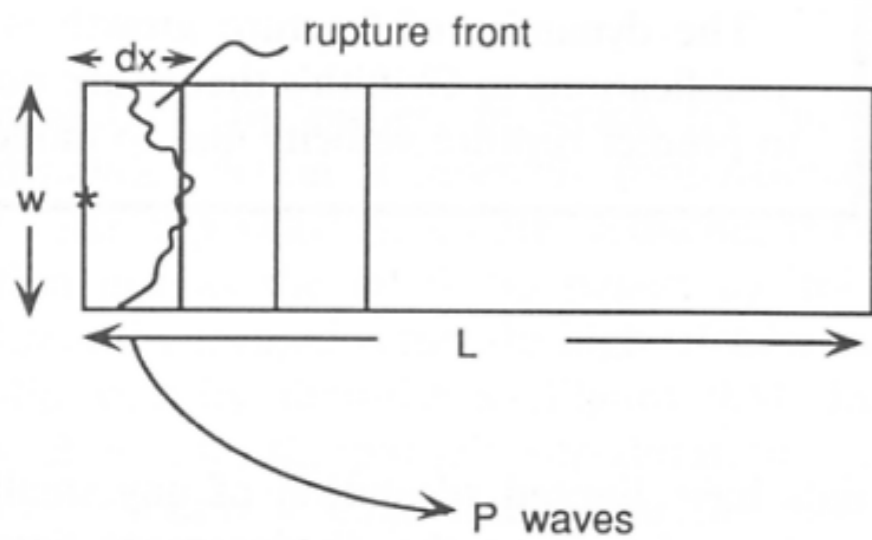


**FIGURE 9.5** Geometry of a one-dimensional fault of width  $w$  and length  $L$ . The individual segments of the fault are of length  $dx$ , and the moment of a segment is  $m dx$ . The fault ruptures with velocity  $v_r$ .

$$\begin{aligned}
 u_r(r, t) &= \sum_{i=1}^N u_i(r_i, t - r_i / \alpha - \Delta t_i) = \\
 &= \frac{R_i^P \mu}{4\pi\rho\alpha^3} W \sum_{i=1}^N \frac{\dot{D}_i}{r_i} (t - \Delta t_i) dx \approx \\
 &\approx \frac{R_i^P \mu}{4\pi\rho\alpha^3} \frac{W}{r} \sum_{i=1}^N \dot{D}(t) * \delta\left(t - \frac{x}{v_r}\right) dx \approx \\
 &\approx \frac{R_i^P \mu}{4\pi\rho\alpha^3} \frac{W}{r} \dot{D}(t) * \int_0^L \delta\left(t - \frac{x}{v_r}\right) dx = \\
 &= \frac{R_i^P \mu}{4\pi\rho\alpha^3} \frac{W}{r} v_r \dot{D}(t) * B(t; T_r)
 \end{aligned}$$

# Haskell source model: far field

$$u_r(r, t) \propto \dot{D}(t) * v_r H(z) \Big|_{t-x/v_r}^t = v_r \dot{D}(t) * B(t; T_r)$$

resulting in the convolution of two boxcars: the first with duration equal to the rise time and the second with duration equal to the **rupture time** ( $L/v_r$ )

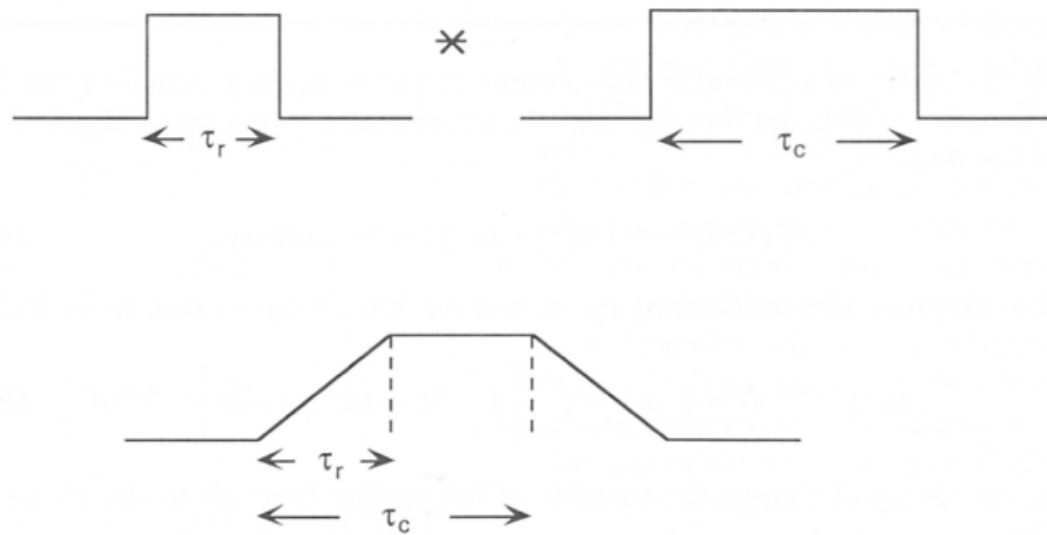


**FIGURE 9.6** The convolution of two boxcars, one of length  $\tau_r$  and the other of length  $\tau_c$  ( $\tau_c > \tau_r$ ). The result is a trapezoid with a rise time of  $\tau_r$ , a top of length  $\tau_c - \tau_r$ , and a fall of width  $\tau_r$ .

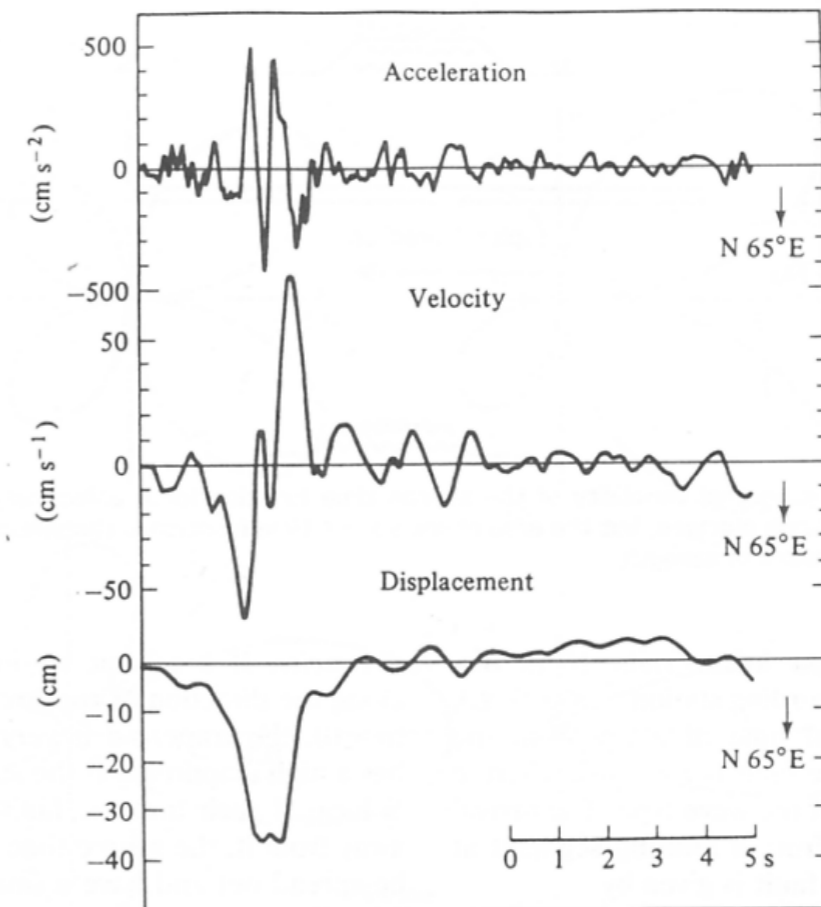
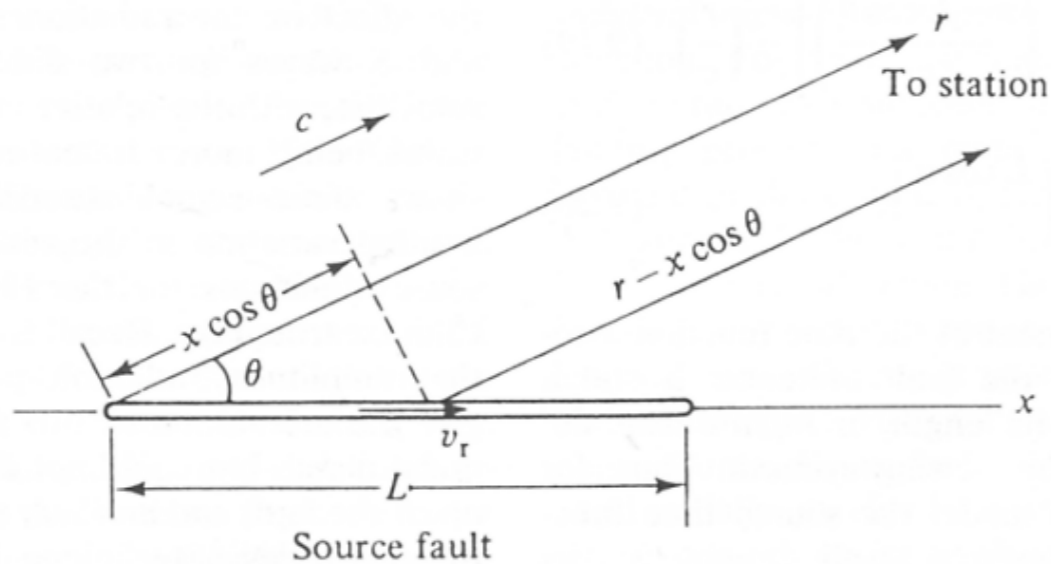


**FIGURE 9.7** A recording of the ground motion near the epicenter of an earthquake at Parkfield, California. The station is located on a node for  $P$  waves and a maximum for  $SH$ . The displacement pulse is the  $SH$  wave. Note the trapezoidal shape. (From Aki, *J. Geophys. Res.* 73, 5359–5375, 1968; © copyright by the American Geophysical Union.)

# Haskell source model: directivity

The body waves generated from a breaking segment will arrive at a receiver before than those that are radiated by a segment that ruptures later.  
 If the path to the station is not perpendicular, the waves generated by different



$$T_r = \left[ \frac{L}{v_r} + \left( \frac{r - L \cos \theta}{c} \right) \right] - \frac{r}{c} =$$

$$= \frac{L}{v_r} - \left( \frac{L \cos \theta}{c} \right) = \frac{L}{v_r} \left( 1 - \frac{v_r}{c} \cos \theta \right)$$

**FIGURE 9.8** Geometry of a rupturing fault and the path to a remote recording station.  
 (From Kasahara, 1981.)

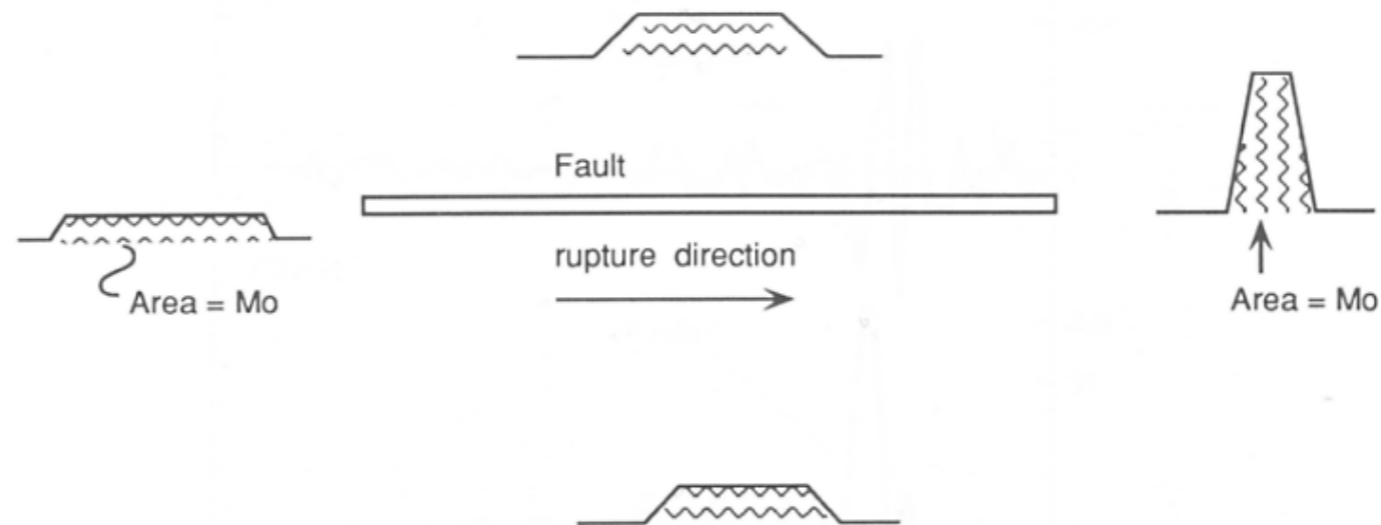


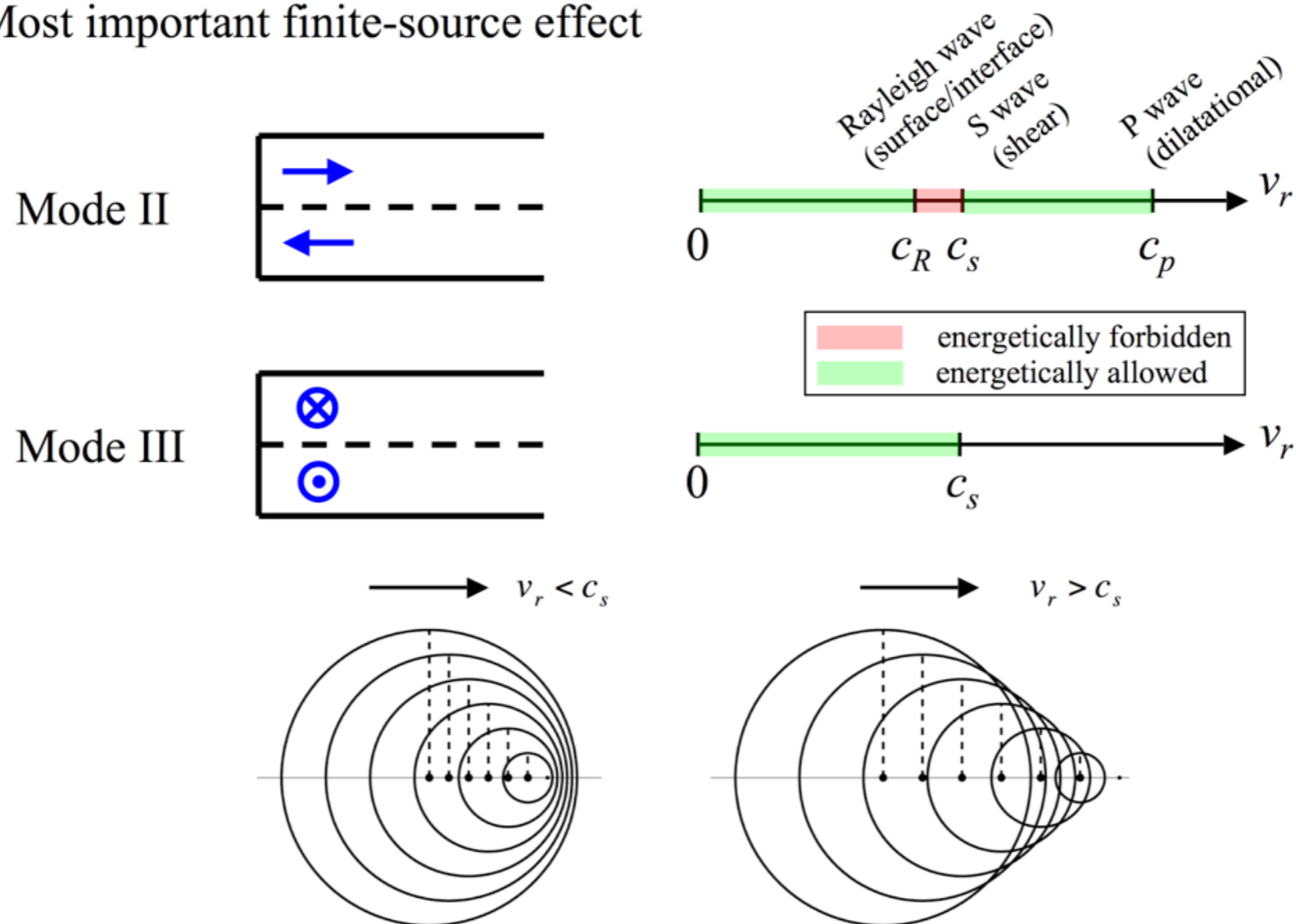
**FIGURE 9.9** Azimuthal variability of the source time function for a unilaterally rupturing fault. The duration changes, but the area of the source time function is the seismic moment and is independent of azimuth.

# Rupture velocity

Earthquake ruptures typically propagate at velocities that are in the range 70-90% of the S-wave velocity and this is independent of earthquake size. A small subset of earthquake ruptures appear to have propagated at speeds greater than the S-wave velocity. These **supershear earthquakes** have all been observed during large strike-slip events.

## Rupture Velocity and Directivity:

Most important finite-source effect



<http://pangea.stanford.edu/~edunham/research/supershear.html>

# Directivity example

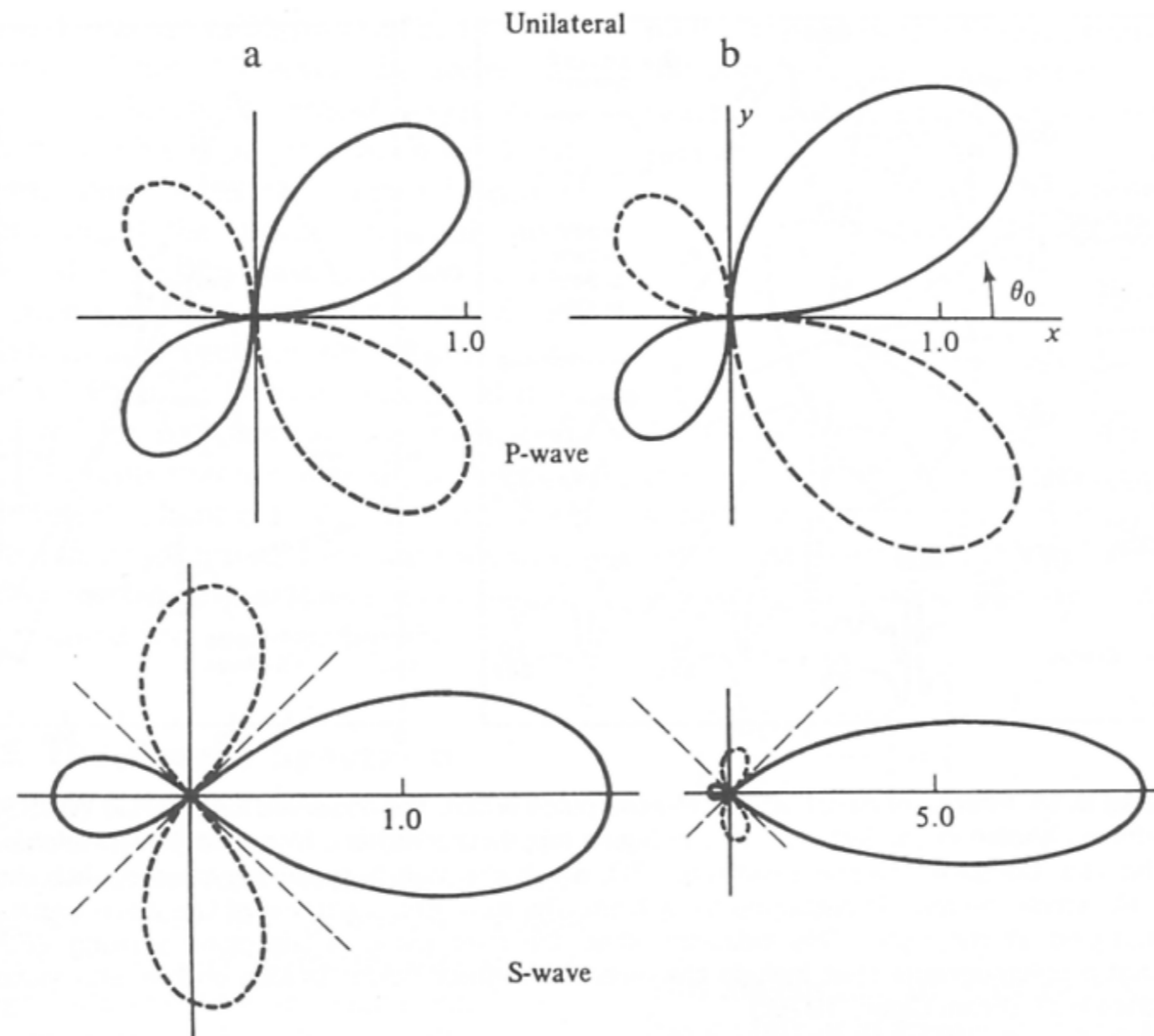


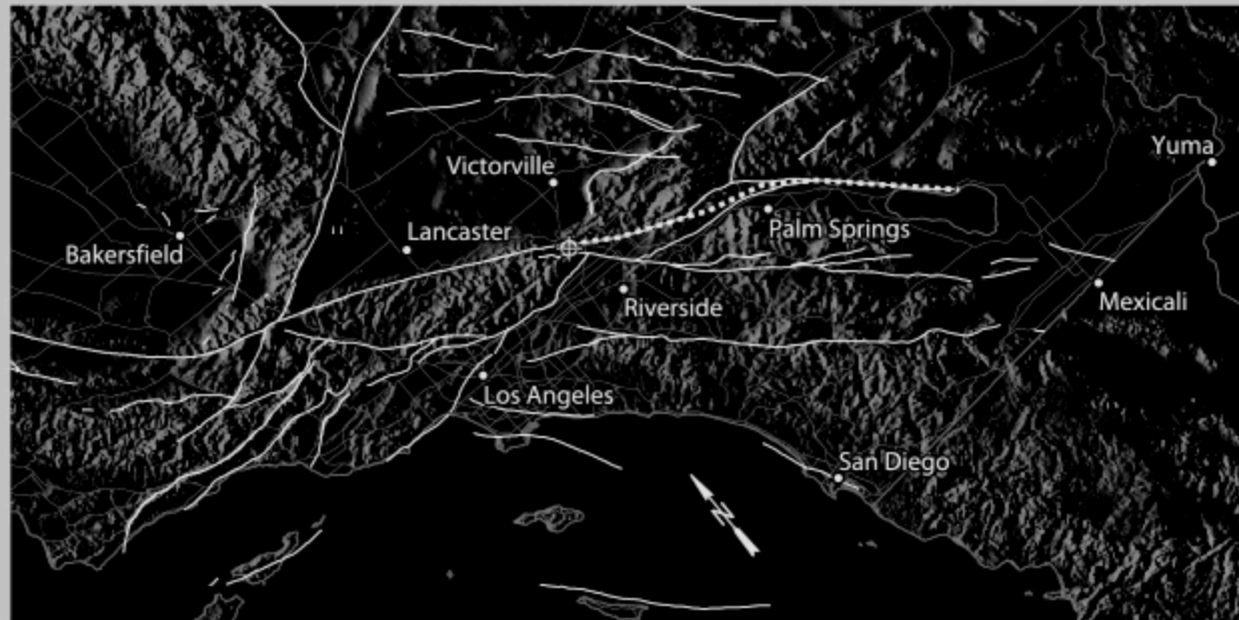
**FIGURE 9.10** The variability of *P*- and *SH*-wave amplitude for a propagating fault (from left to right). For the column on the left  $v_r/v_s = 0.5$ , while for the column on the right  $v_r/v_s = 0.9$ . Note that the effects are amplified as rupture velocity approaches the propagation velocity. (From Kasahara, 1981.)

# Ground motion scenarios

Surface Cumulative Peak Velocity Magnitude ( 2 sec)

■ PeakVelocity:0.0000 Lat:-117.4700 Long:34.2536

■ PeakVelocity:0.0000 Lat:-115.6870 Long:33.3602



Simulation2 (NW-SE)



100 km

Simulation3 (SE-NW)

The two views in this movie show the cumulative velocities for a San Andreas earthquake TeraShake simulation, rupturing south to north and north to south. The crosshairs pinpoint the peak velocity magnitude as the simulation progresses.

[www.scec.org](http://www.scec.org)

# Source spectrum

The displacement pulse, corrected for the geometrical spreading and the radiation pattern can be written as:

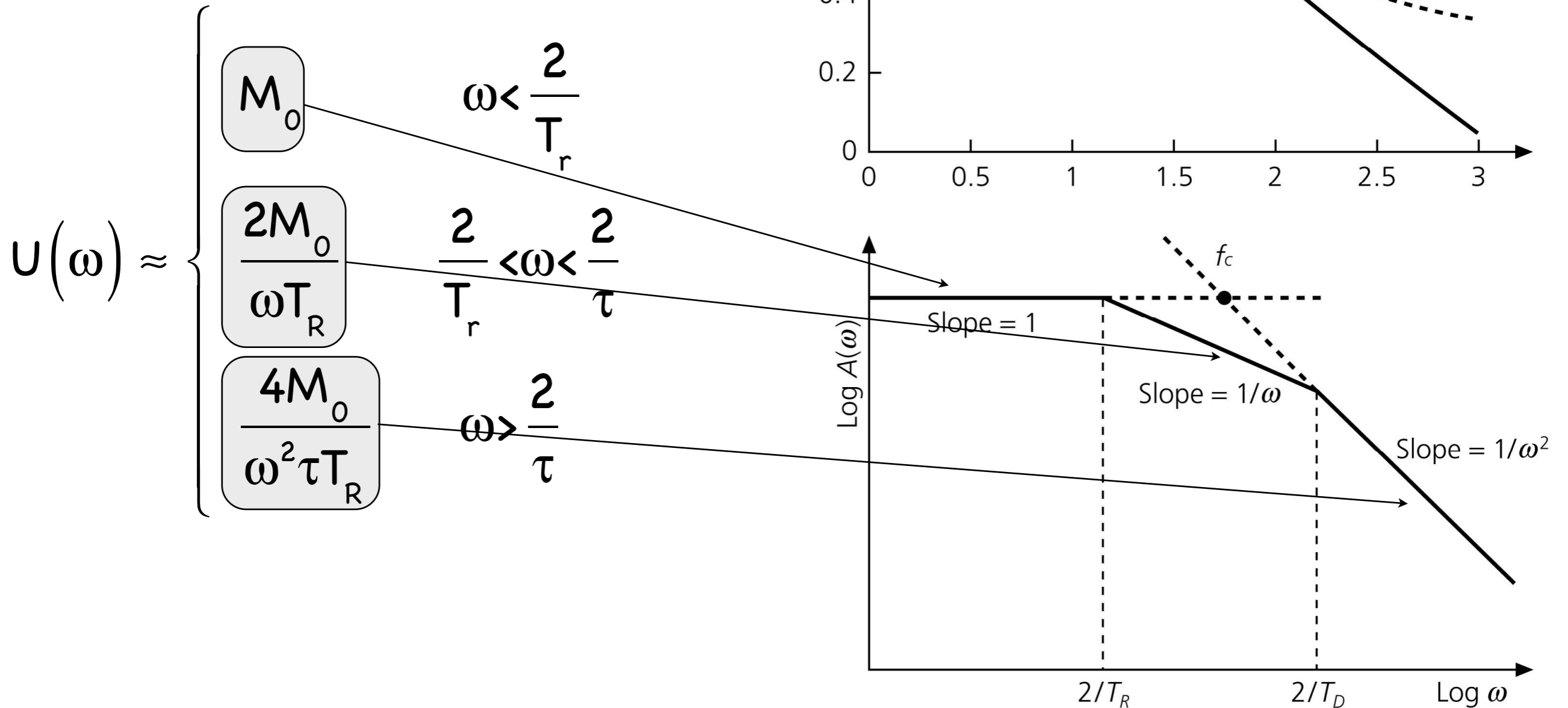
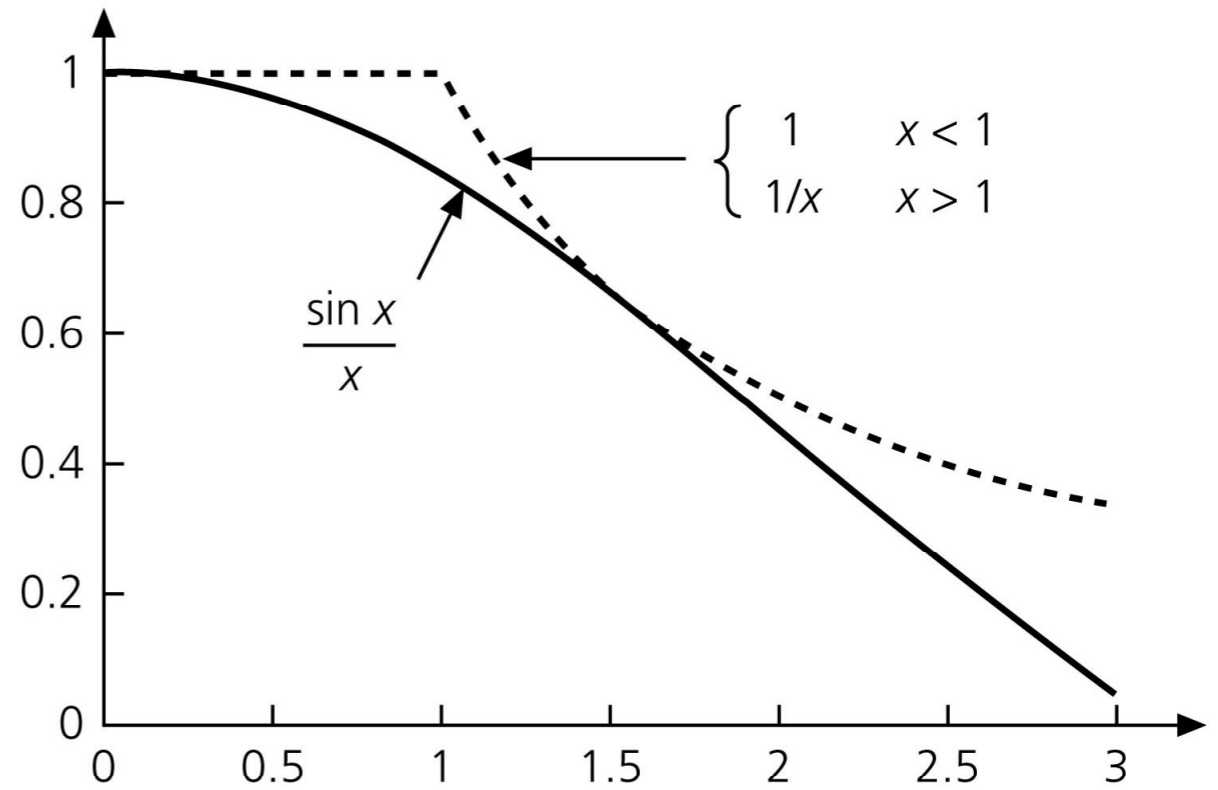
$$u(t) = M_0 \left[ B(t; \tau) * B(t; T_R) \right]$$

and in the frequency domain:

$$\left| U(\omega) \right| = M_0 \left| F(\omega) \right| = M_0 \left| \frac{\sin\left(\frac{\omega\tau}{2}\right)}{\left(\frac{\omega\tau}{2}\right)} \right| \left| \frac{\sin\left(\frac{\omega L}{v_r 2}\right)}{\left(\frac{\omega L}{v_r 2}\right)} \right| \approx \begin{cases} M_0 & \omega < \frac{2}{T_r} \\ \frac{2M_0}{\omega T_R} & \frac{2}{T_r} < \omega < \frac{2}{\tau} \\ \frac{4M_0}{\omega^2 \tau T_R} & \omega > \frac{2}{\tau} \end{cases}$$

# Source spectrum

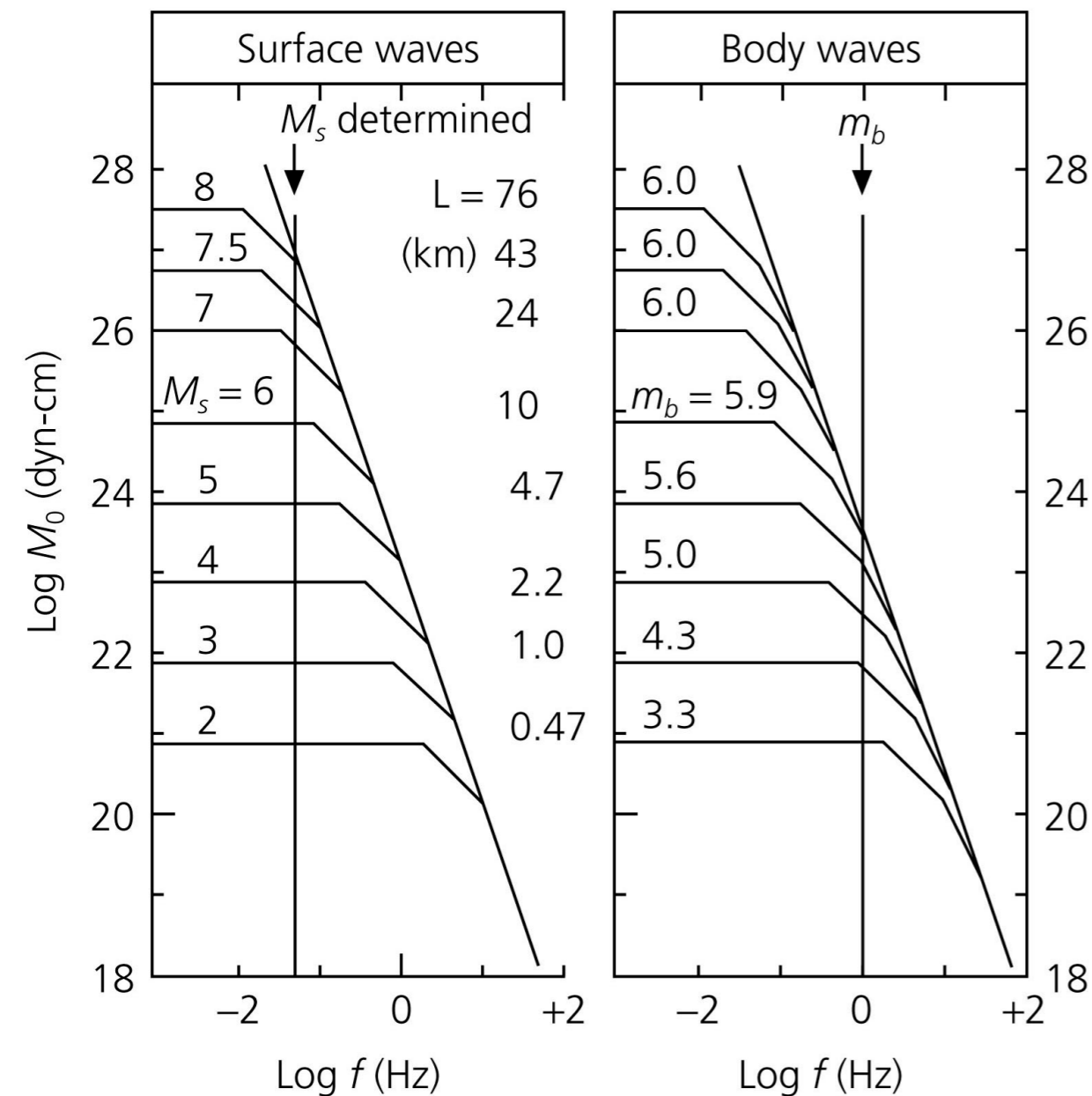
Figure 4.6-4: Approximation of the  $(\sin x)/x$  function, and derivation of corner frequencies.





# Magnitude saturation

Nature limits the maximum size of tectonic earthquakes which is controlled by the maximum size of a brittle fracture in the lithosphere. A simple seismic shear source with linear rupture propagation has a typical "source spectrum".



$M_s$  is not linearly scaled with  $M_0$  for  $M_s > 6$  due to the beginning of the so-called saturation effect for spectral amplitudes with frequencies  $f > f_c$ . This saturation occurs already much earlier for  $m_b$  which are determined from amplitude measurements around 1 Hz.